PTEP

Prog. Theor. Exp. Phys. **2022** 043A01(27 pages)
DOI: 10.1093/ptep/ptac045

Emergence of Lie group symmetric classical spacetimes in the canonical tensor model

Taigen Kawano and Naoki Sasakura*

Yukawa Institute for Theoretical Physics, Kyoto University, Kitashirakawa, Sakyo-ku, Kyoto 606-8502, Japan

*E-mail: sasakura@yukawa.kyoto-u.ac.jp

Received September 29, 2021; Revised January 31, 2022; Accepted March 9, 2022; Published March 11, 2022

We analyze a wave function of a tensor model in the canonical formalism, when the argument of the wave function takes Lie group invariant or nearby values. Numerical computations show that there are two phases, which we call the quantum and the classical phases. In the classical phase fluctuations are suppressed, and configurations emerge which are discretizations of classical geometric spaces invariant under Lie group symmetries. This is explicitly demonstrated for emergence of S^n ($n = 1, 2, 3$) for $SO(n+1)$ symmetries by checking the topological and geometric (Laplacian) properties of the emerging configurations. The transition between the two phases has the form of splitting/merging of distributions of variables, resembling a matrix model counterpart, namely the transition between one-cut and two-cut solutions. However, this resemblance is obscured by a difference in the mechanism of distribution in our setup from that in the matrix model. We also discuss this transition as a replica symmetry breaking. We perform various preliminary studies of the properties of the phases and the transition for such values of the argument.

Subject Index A13, A22, E05

1. Introduction

Lie groups [1] are ubiquitous in spacetime. Fundamental interactions are disciplined by Lie group gauge symmetries, Lorentz symmetry constrains the spacetime structure of theories, and de Sitter symmetry is globally realized in the Universe. Therefore, when we think of emergence of spacetimes in quantum gravity [2–15], it would be natural to think of emergence of Lie group symmetries at the same time, or even consider them as different aspects of one phenomenon.

In this paper we discuss a tensor model in the Hamiltonian formalism from the perspective above. Tensor models [11–14] were originally introduced as a generalization of the matrix model, which successfully describes two-dimensional quantum gravity, to higher dimensions. However, tensor models were shown to suffer from dominance of singular spaces [16,17], which makes it difficult to generate globally extended spaces. Hoping to improve the issue, one of the present authors introduced a new type of tensor model with a time direction [15,18], which we call the canonical tensor model (CTM). CTM incorporates an analogue of the spacetime diffeomorphism invariance, which is a fundamental in general relativity, by mimicking the structure of the Hamiltonian formalism of general relativity (more precisely, the Arnowitt–Deser–Misner (ADM) formalism [19]). The reason we think introducing time may improve the difficulty comes from the success of causal dynamical triangulation [20] over dynamical triangulation in the emergence of globally extended spacetimes, where the former is a dynamical lattice

© The Author(s) 2022. Published by Oxford University Press on behalf of the Physical Society of Japan.
This is an Open Access article distributed under the terms of the Creative Commons Attribution License (https://creativecommons.org/licenses/by/4.0/), which permits unrestricted reuse, distribution, and reproduction in any medium, provided the original work is properly cited.
Funded by SCOAP[3]

Downloaded from https://academic.oup.com/ptep/article/2022/4/043A01/6547023 by Kyoto Daigaku Nogaku-bu Toshoshitsu user on 23 January 2023

formulation of quantum gravity with a time direction, but the latter is one without it. It would be a highly interesting question whether or not CTM enjoys similar success. From previous studies [21,22], it is known that the wave function $\Psi(P)$ of CTM has peaks at Lie group invariant Ps, where P denotes one of the canonically conjugate pair of the dynamical variables (tensors) of CTM.[1] This peak–Lie group relation implies that Lie group invariant configurations are favored, or in other words, Lie group symmetries emerge in CTM. Then, from the perspective mentioned in the first paragraph, the question is whether this can be linked to emergence of spacetimes. We show that this can be seen in $\Psi(Q)$, which is the wave function representing the same state in the other variable, Q, conjugate to P.

The most important difference of this paper from the previous similar study [23] of $\Psi(Q)$ is the discovery of a new phase, which we call the classical phase in this paper. Fluctuations of variables are suppressed in this phase, and configurations emerge which are discretizations of classical geometric spaces. This will explicitly be demonstrated for n-dimensional spheres S^n ($n = 1, 2, 3$) by computing the wave function $\Psi(Q)$ for Q taking $SO(n+1)$ invariant or nearby values by applying the Hamiltonian Monte Carlo method.

As we will see later, the transition to the classical phase has a striking resemblance to a matrix counterpart, which is the transition from one-cut to two-cut solutions in the large-N limit of the matrix model [24], or the Gross–Witten–Wadia-type transition [25,26]. In fact, in Ref. [27] a two-logarithm matrix model which is a matrix analogue to the wave function of CTM was analyzed, and it was shown that transitions exist from one-cut to two-cut solutions where certain dimensional cloud-like configurations emerge. Though these configurations of certain dimensions are hard to regard as spaces with classical geometry, it is interesting that we find a common phenomenon in the matrix and the tensor models.

As discussed later, we want to stress the importance of the positivity of the cosmological constant of CTM taken in this paper (see Appendix A about the cosmological constant in CTM). When it is positive, the wave function is expressed by an oscillatory integration that generally suppresses the configurations in the quantum phase due to cancellations, compared to those in the classical phase. Therefore, the positivity is essential for the emergence of classical geometric spaces in the classical phase.

Obviously, the next question from the result of this paper would be whether the emergent classical geometric spaces follow the equations of general relativity. We would like to stress that there is a good chance for this to be shown in a future study. First of all, CTM is formulated as a first-class constraints system which has a very similar structure to ADM (see Appendix A for more details) [15,18]. In fact, in a formal continuum limit,[2] the constraint algebra of CTM agrees with that of ADM [28]. More explicitly, in the formal continuum limit, the classical equation of motion of P in CTM agrees with the Hamilton–Jacobi equation of general relativity with a Hamilton's principal function of a local form [29]. We can also add that the $N = 1$ case of CTM agrees with the mini-superspace approximation of general relativity [30].

This paper is organized as follows. In Sect. 2 we explain the setup, namely the wave function of CTM we analyze. In Sect. 3 we explain the Monte Carlo method we employ, namely the reweighting method applied to the wave function. In Sect. 4 we explain how to construct the

[1] The dynamical variables of CTM are a canonical conjugate pair of real symmetric three-index tensors, Q_{abc} and P_{abc} ($a, b, c = 1, 2, \ldots, N$). See Appendix A for more about CTM.

[2] This formal limit is analogous to formally taking the vanishing limit of a lattice size in a lattice theory without considering its dynamics.

Downloaded from https://academic.oup.com/ptep/article/2022/4/043A01/6547023 by Kyoto Daigaku Nogaku-bu Toshoshitsu user on 23 January 2023

Lie group invariant values of Q we take as the argument of the wave function. We consider $SO(n+1)\,(n=1,2,3)$ as the Lie groups, and take some natural sets of representations on Q. In Sect. 5 we show the presence of two phases, the quantum and the classical phases, by the Monte Carlo method. We observe the transition where the topology of the distributions of the variables continuously changes between one bunch in the quantum phase and two bunches in the classical phase. In the classical phase, the fluctuations of the variables are suppressed. In Sect. 6 we discuss the translation between geometry and a real symmetric three-index tensor through the tensor rank decomposition. In particular, we define a discrete analogue of the Laplacian, which is used to analyze the geometry of emerging configurations in the classical phase. In Sect. 7 we study the topology and the geometry of the emerging configurations in the classical phase. We find S^n for $SO(n+1)\,(n=1,2,3)$ invariant Q. In Sect. 8 we consider two kinds of deformations of Q from those given in Sect. 4. One is to change the representations on Q, and the other is to break the Lie group invariance. In both cases, we find the classical phase becomes less likely by the deformations. In Sect. 9 we study the behavior of the complex part in the reweighting method in some detail. Because of the positivity of the cosmological constant, the configurations in the quantum phase are generally suppressed due to cancellations, compared to those in the classical phase. This suppression is enhanced for larger $|Q|$, and the main physical statement is that the system starts from the quantum phase with small $|Q|$, and undergoes the transition to the classical phase as $|Q|$ develops. This suggests that $|Q|$ can be naturally identified as a time direction in CTM. The last section is devoted to a summary and future prospects.

2. The wave function

In this section we explain the setup of the wave function we will analyze, leaving some details to Appendix A.

The canonical tensor model [15,18] is a tensor model in the canonical formalism, formulated in the analogue of the ADM formalism [19] of general relativity. The motivation for the formulation is to incorporate a time direction consistently with the fundamental of general relativity, namely, the general covariance. The quantized Hamiltonian [31] of CTM is given by

$$\hat{H} = N_a \hat{H}_a + N_{[ab]} \hat{J}_{[ab]}, \tag{1}$$

where $\hat{H}_a$ and $\hat{J}_{[ab]}$ are the quantized Hamiltonian and the momentum constraints of CTM, and N_a and $N_{[ab]}$ are the lapse and the shift parameters, respectively. Repeated lower indices are assumed to be summed over throughout this paper. The commutation algebra between the quantized constraints is non-linearly closed, making them first-class constraints. The physical state condition is given by the CTM analogue of the Wheeler–DeWitt equation [32],

$$\hat{H}_a |\Psi\rangle = 0, \tag{2}$$

accompanied by $\hat{J}_{[ab]}|\Psi\rangle = 0$. An explicit solution to these equations for general N exists [33], and the wave function in the P-representation is given by an integral expression,

$$\Psi(P) := \langle P|\Psi\rangle = \int_{\mathcal{C}} d\phi\, d\tilde{\phi}\, \exp\left[i \sum_{j=1}^{R} \left(P(\phi^j)^3 - (\phi^j)^2 \tilde{\phi}^j + (\tilde{\phi}^j)^3/3 \right) \right], \tag{3}$$

Downloaded from https://academic.oup.com/ptep/article/2022/4/043A01/6547023 by Kyoto Daigaku Nogaku-bu Toshoshitsu user on 23 January 2023

where the integration variables are ϕ_a^j, $\tilde{\phi}^j$ ($a = 1, 2, \ldots, N, j = 1, 2, \ldots, R$), and

$$d\phi\, d\tilde{\phi} := \prod_{j=1}^{R} d\tilde{\phi}^j \prod_{a=1}^{N} d\phi_a^j, \qquad P(\phi^j)^3 := P_{abc}\phi_a^j\phi_b^j\phi_c^j, \qquad (\phi^j)^2 := \phi_a^j\phi_a^j. \tag{4}$$

Summations over the upper indices (namely, j above) are explicitly indicated throughout this paper. The parameter R is restricted to be $R = (N + 2)(N + 3)/4$, which comes from the hermiticity of the Hamiltonian constraint $\hat{H}_a$ [31]. In the expression in Eq. (3), R serves as the replica number of the set $(\phi_a^j, \tilde{\phi}^j)$, and the possible values of N are restricted for R to be an integer. However, we would be able to assume that small deviations of R would not largely change the dynamics of our Monte Carlo simulations, and will take

$$R = \lfloor (N + 2)(N + 3)/4 \rfloor, \tag{5}$$

where $\lfloor \cdot \rfloor$ denotes the floor function, allowing any values of N. In Eq. (3), we have taken a positive value[3]for the cosmological constant of CTM [30], since the positivity is essential for the peak–Lie group symmetry relation [21,22] mentioned in Sect. 1. In the positive case, the second term in the exponent of Eq. (3) takes the minus sign as shown there, generating the Airy function dependence Airy$(-(\phi^j)^2)$ (see Appendix A for more details), which is oscillatory and essential in later sections. As for the integration region $\mathcal{C}$, we take the integration region of ϕ to be the real numbers $\mathbb{R}^{NR}$,[4]and the integration contour of $\tilde{\phi}$ will be specified in Sect. 3.

The wave function in the Q-representation can be obtained by the Fourier transformation of $\Psi(P)$ in Eq. (3). However, this generates a product of delta functions because the exponent of the integrand is linear in P. This delta function product is difficult to handle in the Monte Carlo method. Therefore, we introduce a regularization term $-P_{abc}P_{abc}/4\lambda$ ($\lambda > 0$) into the exponent, and then we obtain

$$\begin{aligned}\Psi(Q, \lambda) &= \int dP d\phi\, d\tilde{\phi}\, e^{iP_{abc}Q_{abc} - P_{abc}P_{abc}/4\lambda}\, \Psi(P) \\ &= \int_{\mathcal{C}} d\phi\, d\tilde{\phi}\, \exp\left[-\lambda\left(Q - \sum_{j=1}^{R}\phi^j\phi^j\phi^j\right)^2 + i\sum_{j=1}^{R}\left(-(\phi^j)^2\tilde{\phi}^j + (\tilde{\phi}^j)^3/3\right)\right],\end{aligned} \tag{6}$$

where we have ignored an inessential overall factor, have performed $\phi \to -\phi$ for convenience, and have introduced the short-hand notation

$$\left(Q - \sum_{j=1}^{R}\phi^j\phi^j\phi^j\right)^2 := \left(Q_{abc} - \sum_{j=1}^{R}\phi_a^j\phi_b^j\phi_c^j\right)\left(Q_{abc} - \sum_{j=1}^{R}\phi_a^j\phi_b^j\phi_c^j\right). \tag{7}$$

In the above, the parameter λ is introduced as a regularization parameter, which changes the wave function. Since the wave function should be a solution to the Wheeler–DeWitt equation, Eq. (2), the physical meaning of $\Psi(Q, \lambda)$ with a finite λ is not clear. Instead, rather than as a regularization, we may introduce λ as part of an observable which operates on $\Psi(q) := \int dP\, e^{iP_{abc}q_{abc}}\, \Psi(P)$, which is the genuine wave function in Q-representation. More precisely, it can be introduced as a smearing operator $\langle q_1|\hat{O}_\lambda|q_2\rangle := e^{-\lambda(q_1-q_2)^2}$ acting on Ψ:

$$\Psi(Q, \lambda) := (\hat{O}_\lambda\Psi)(Q) = \int dq\, e^{-\lambda(Q-q)^2}\Psi(q), \tag{8}$$

[3]Namely, $\Lambda_c = 4/9$. See Appendix A for more details.

[4]The integration region must be deformed slightly from the real values to make the integration convergent, or a regularization must be introduced as in Ref. [21]. A mathematically rigorous way to define the integration contour can be provided by the Lefschetz thimble [34].

Downloaded from https://academic.oup.com/ptep/article/2022/4/043A01/6547023 by Kyoto Daigaku Nogaku-bu Toshoshitsu user on 23 January 2023

which has the same form as Eq. (6) up to an irrelevant normalization.

In the first way of introducing λ above, it must be taken infinitely large to remove the regularization. In the second, it is not necessary to take it infinitely large, but, as we will see later, the coupling λ is effectively given by $\lambda|Q|^2$. This means that the coupling must be taken larger as spacetime develops.[5] However, we consider only the range $\lambda \lesssim 10^7$ in this paper, which comes from the technical reason that our Monte Carlo simulation becomes inefficient above this value.

It is worth commenting on the convergence of Eq. (6). The sum $\sum_{i=1}^{R} \phi_a^i \phi_b^i \phi_c^i$ in Eq. (6) has a lot of flat directions to infinity of ϕ, such as the one with $\phi_a^i \phi_b^i \phi_c^i + \phi_a^j \phi_b^j \phi_c^j = 0$ $(i \neq j)$ by taking $\phi^i = -\phi^j$. It is therefore generally a non-trivial matter whether or not the integral in Eq. (6) converges. The convergence for $R \lesssim N^2/2$ was first noticed in Ref. [35], and was more systematically analyzed in Ref. [36]. Since our value of R in Eq. (5) is roughly smaller by a factor of 2, the current analysis does not suffer from the divergence, which indeed was checked in our actual Monte Carlo simulations.

3. The Monte Carlo method

We want to evaluate Eq. (6) by the Monte Carlo method. However, the integrand contains an oscillatory part, i.e. Eq. (6) suffers from the notorious sign problem [37]. To deal with this issue we take the most naive method, the so-called reweighting method. Though more sophisticated methods exist, it would be appropriate to apply this simple method to the current primary study of the system, since it is difficult to foresee potential complications caused by the other more sophisticated methods.

As we mentioned earlier, the integration contour is taken to be $\mathcal{C} = \mathbb{R}^{NR} \times \tilde{\mathcal{C}}^R$, where the former is for ϕ and the latter for $\tilde{\phi}$. Then we rewrite Eq. (6) as

$$\Psi(Q,\lambda) = Z_{Q,\lambda} \left\langle \int_{\tilde{C}} d\tilde{\phi}\, e^{i\sum_{j=1}^{R}\left(-(\phi^j)^2\tilde{\phi}^j + (\tilde{\phi}^j)^3/3\right)} \right\rangle_{Q,\lambda}, \tag{9}$$

where

$$Z_{Q,\lambda} = \int_{\mathbb{R}^{NR}} d\phi\, e^{-\lambda\left(Q - \sum_{j=1}^{R}\phi^j\phi^j\phi^j\right)^2}, \tag{10}$$

and the expectation value $\langle\, \cdot\, \rangle$ is taken for the system defined by the partition function in Eq. (10). The expression becomes more convenient for actual Monte Carlo simulations by splitting the size of Q as $Q_{abc} = |Q|\tilde{Q}_{abc}$, where $|Q| := \sqrt{Q_{abc}Q_{abc}}$, and performing the rescaling $\phi \to |Q|^{1/3}\phi$:

$$\Psi(Q,\lambda) = |Q|^{NR/3}\, Z_{\tilde{Q},\lambda|Q|^2} \left\langle \prod_{j=1}^{R} \mathrm{Airy}\left(-|Q|^{2/3}(\phi^j)^2\right) \right\rangle_{\tilde{Q},\lambda|Q|^2}, \tag{11}$$

where we have used the integral expression of the Airy function,

$$\mathrm{Airy}(-z) = \int_{\tilde{C}} d\tilde{\phi}\, e^{i\left(-z\tilde{\phi} + \tilde{\phi}^3/3\right)}. \tag{12}$$

Note that our interest is only the positive region $z \geq 0$ as in Eq. (11). A natural choice of the Airy function for the current study is given by setting

$$\mathrm{Airy}(-z) = \mathrm{Ai}(-z) + i\,\mathrm{Bi}(-z), \tag{13}$$

since this function asymptotically approaches a plane wave form (see Fig. 1). This choice cor-

[5] We assume here that $|Q|$ is correlated with time, as Q is proportional to the spatial volume in the agreement of the $N = 1$ CTM with the mini-superspace approximation of general relativity [30].

Downloaded from https://academic.oup.com/ptep/article/2022/4/043A01/6547023 by Kyoto Daigaku Nogaku-bu Toshoshitsu user on 23 January 2023

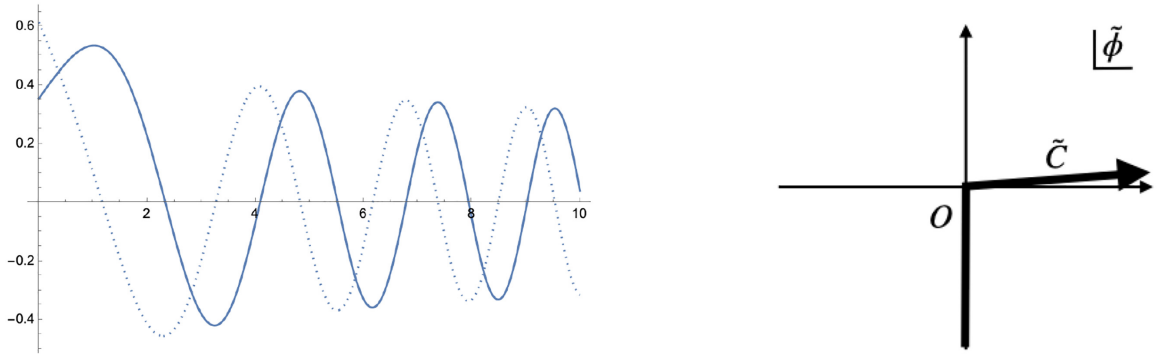

Fig. 1. Left: The plot of Eq. (13) against z. The solid and dashed lines represent the real and imaginary parts, respectively. Right: The integration contour $\tilde{C}$, slightly deformed from the real axis for $\tilde{\phi} > 0$.

responds to the integration contour $\tilde{C}$ to be taken as in the right panel of Fig. 1. From Eq. (11), we see that it is enough to compute $Z_{Q,\lambda}$ and $\langle \cdot \rangle_{Q,\lambda}$ for $|Q| = 1$, which we will carry out in later sections.

We employ the Hamiltonian Monte Carlo method [38] to generate the sampling sequence of ϕ_a^j ($a = 1, 2, \ldots, N, j = 1, 2, \ldots, R$) for the system defined by Eq. (10). The leapfrog numbers are typically taken with a few hundreds depending on the sizes of N, R. We also use parallel tempering [39] across different values of λ for a difficult case (more concretely, the $SO(4)$ case with $N = 30$ and $R = 264$, which will appear later). The total numbers of samples for each sequence are typically around $10^4 \sim 10^6$. As for the analyzed data, one data is taken from every $\sim 10^2$ samples to remove correlations. The machine has a Xeon W2295 processor (3.0 GHz, 18 cores), 128 GB DDR4 memory, and runs the Ubuntu 20 operating system. The program is written in C++ using pthreads for parallelization. As for the Airy function, the Boost library [40] is used. Every run typically takes several hours with active use of parallelization.

Lastly, we want to stress the importance of taking the cosmological constant of CTM to be positive in our setup. In this case, the Airy function is oscillatory, as is taken above, and this oscillatory property plays the very important role of highlighting the configurations in the classical phase, as discussed in Sect. 9. On the other hand, if the cosmological constant is taken negative, Airy(z) with $z = (\phi^j)^2$ appears instead, which is given by a linear combination of the two Airy functions Ai(z) and Bi(z). They are asymptotically exponential,[6] and the only possible choice will be Airy(z) = Ai(z) to avoid divergence as $z \to \infty$. Now Ai(z) is a monotonic damping function, and does not discriminate the configurations in the classical phase from those in the quantum phase. In fact, in Refs. [35,41,42], the wave function in the negative cosmological constant case was analyzed with an approximation to the Airy function part, but no signs of emerging classical geometric spaces have been found.

4. Construction of Lie group invariant Q

Various ways exist to construct Lie group invariant Q. We employ the construction using harmonic functions on Lie group invariant manifolds [43], with the expectation of the emergence of space-like objects from the wave function in Eq. (6) for such Q. Some deformations from such Q will also be considered in Sect. 8.

[6] They behave as $\mathrm{Ai}(z) \sim e^{-2z^{3/2}/3}$ and $\mathrm{Bi}(z) \sim e^{2z^{3/2}/3}$ for $z \to +\infty$.

Downloaded from https://academic.oup.com/ptep/article/2022/4/043A01/6547023 by Kyoto Daigaku Nogaku-bu Toshoshitsu user on 23 January 2023

We consider three Lie groups here, $SO(n+1)$ $(n = 1, 2, 3)$. The manifolds we expect to emerge are S^n.

4.1. *SO(2) invariant Q*

The harmonic functions on S^1 are given by

$$\{f_a(\theta)\} = \{1/\sqrt{2}\} \cup \{\cos(p\theta), \sin(p\theta) \mid p = 1, 2, \ldots, \Lambda\}, \tag{14}$$

with $\theta \in [0, 2\pi)$, where Λ denotes a cut-off of the momentum. There are $N = 2\Lambda + 1$ functions in total. Then an invariant tensor Q is constructed by

$$Q^{SO(2)}_{abc}(\alpha) = \text{const.}\, e^{-\alpha(p_a^2+p_b^2+p_c^2)/\Lambda^2} \int_0^{2\pi} d\theta\, f_a(\theta) f_b(\theta) f_c(\theta), \tag{15}$$

where p_a denotes the momentum of the function f_a (i.e. p_a for $f_a = \cos(p_a\theta)$, $\sin(p_a\theta)$); const. is a normalization factor for $|Q^{SO(2)}(\alpha)| = 1$. The exponential factor introduces a smooth momentum cut-off, and larger α would effectively make S^1 smaller, since the number of functions is effectively reduced. A negative α would also be possible but a space represented by such an α would be pathological.

4.2. *SO(3) invariant Q*

The harmonic functions on S^2 are the spherical harmonics $Y_l^m(\omega)$, where ω is a coordinate system on S^2. Similarly, we consider

$$\{f_a\} = \{\text{Re}\, Y_l^m(\omega), \text{Im}\, Y_l^m(\omega) \mid l = 0, 1, \ldots, \Lambda,\ m = -l, -l+1, \ldots, l\}, \tag{16}$$

where vanishing and degenerate functions are supposed to be discarded (e.g. Im $Y_l^0 = 0$). There are a total of $N = (\Lambda + 1)^2$ independent functions. Then we define[7]

$$Q^{SO(3)}_{abc}(\alpha) = \text{const.}\, e^{-\alpha(l_a^2+l_b^2+l_c^2)/\Lambda^2} \int_{S^2} d^2\omega\, f_a(\omega) f_b(\omega) f_c(\omega), \tag{17}$$

where const. is a normalization factor for $|Q^{SO(3)}(\alpha)| = 1$.

4.3. *SO(d + 1) invariant Q*

The harmonic functions on S^d are $Y_{m,l_1,\ldots,l_{d-1}}(\omega)$, where $(\omega^i) = (\varphi, \theta_1, \ldots, \theta_{d-1})$ is a spherical coordinate system on S^d. Similarly, we consider

$$\{f_a\} = \{Y_{m,l_1,\ldots,l_{d-1}} \mid m \in \mathbb{Z},\ l_i \in \mathbb{Z}_{\geq 0},\ |m| \leq l_1 \leq l_2 \leq \cdots \leq l_{d-1} \leq \Lambda\}. \tag{18}$$

An iterative way of constructing $Y_{m,l_1,\ldots,l_{d-1}}(\omega)$ is given as follows [44]: given the harmonic functions $Y_{m,l_1,\ldots,l_{d-2}}(\varphi, \theta_1, \ldots, \theta_{d-2})$ on S^{d-1}, the harmonic functions on S^d are defined by

$$Y_{m,l_1,\ldots,l_{d-1}}(\varphi, \theta_1, \ldots, \theta_{d-1}) = B^d_{l_{d-1},l_{d-2}}(\theta_{d-1})\, Y_{m,l_1,\ldots,l_{d-2}}(\varphi, \theta_1, \ldots, \theta_{d-2}), \tag{19}$$

where

$$B^d_{l_{d-1},l_{d-2}}(\theta) := \left(\frac{\left(l_{d-1} + \frac{d-1}{2}\right)(l_{d-1} + l_{d-2} + d - 2)!}{(l_{d-1} - l_{d-2})!} \right)^{\frac{1}{2}} (\sin\theta)^{1-\frac{d}{2}} P^{-l_{d-2}+1-\frac{d}{2}}_{l_{d-1}-1+\frac{d}{2}}(\cos\theta), \tag{20}$$

with the Legendre function P. The derivation is summarized in Ref. B. Since harmonic functions satisfy the Helmholtz equation,

$$-\Delta Y_{m,l_1,\ldots,l_{d-1}} = l_{d-1}(l_{d-1} + d - 1) Y_{m,l_1,\ldots,l_{d-1}}, \tag{21}$$

[7]The l dependence of the regularization term can be taken differently, like using the eigenvalues of the Laplacian instead. But such details would not affect the essential results as far as the regularization is a smooth damping function invariant under the Lie group. Otherwise, the results cannot be considered universal.

Downloaded from https://academic.oup.com/ptep/article/2022/4/043A01/6547023 by Kyoto Daigaku Nogaku-bu Toshoshitsu user on 23 January 2023

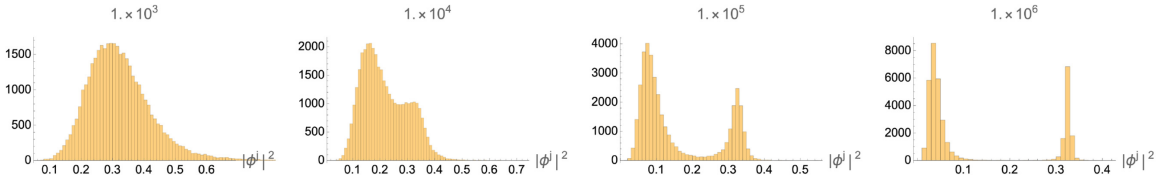

Fig. 2. Histograms of $|\phi^j|^2$ for $Q^{SO(2)}$ with $N = 15$ ($\Lambda = 7$) and $\alpha = 0.5$. The data are the collection of $|\phi^j|^2$ ($j = 1, 2, \ldots, R$) over the sampled data of the Monte Carlo simulations. The values of λ are shown over each figure. The classical phase can be found for $\lambda \gtrsim 10^6$.

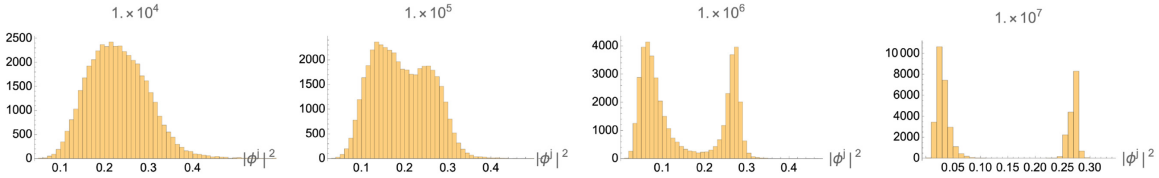

Fig. 3. Histograms for $Q^{SO(3)}$ with $N = 16$ ($\Lambda = 3$) and $\alpha = 0.5$, plotted as in Fig. 2. The classical phase can be found for $\lambda \gtrsim 10^7$.

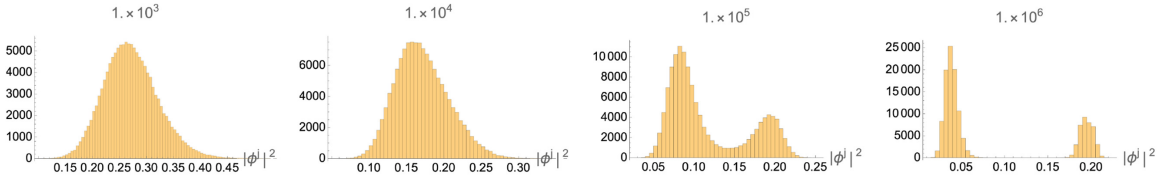

Fig. 4. Histograms for $Q^{SO(4)}$ with $N = 30$ ($\Lambda = 3$) and $\alpha = 0.5$, plotted as in Fig. 2. The classical phase can be found for $\lambda \gtrsim 10^6$. On the other hand, the $\Lambda = 2$ case does not show the presence of the classical phase up to $\lambda \leq 10^7$.

with the Laplacian Δ, the eigenvalue associated with $f_a = Y_{m,l_1,\ldots,l_{d-1}}$ is $e_a = l_{d-1}(l_{d-1} + d - 1)$. The total number of independent functions is $N = [\Lambda^{\bar{d}} + (\Lambda+1)^{\bar{d}}]/d!$, where $x^{\bar{n}} = x(x+1)\cdots(x+n-1)$ is the rising factorial.

Now let us look at the case where $d = 3$. Since Y_l^m in the standard notation corresponds to $Y_{m,l}$ in the case of $d = 2$, the subset of harmonic functions on S^3 is

$$\{f_a\} = \{B^3_{k,l}(\chi)\, Y_l^m(\varphi,\theta) \mid m \in \mathbb{Z},\ l,k \in \mathbb{Z}_{\geq 0},\ |m| \leq l \leq k \leq \Lambda\}. \tag{22}$$

The cardinality of the set is $N = (\Lambda+1)(\Lambda+2)(2\Lambda+3)/6$. Then we define

$$Q^{SO(4)}_{abc}(\alpha) = \text{const.}\, e^{-\alpha(e_a+e_b+e_c)/e_\Lambda} \int_{S^3} d^3\omega\, f_a(\omega) f_b(\omega) f_c(\omega), \tag{23}$$

where const. is a normalization factor for $|Q^{SO(4)}(\alpha)| = 1$. To do this calculation we used the Mathematica package HFT11 [45]. This package can enumerate a system of orthogonal functions on S^d as a function of a unit vector $\hat{x} \in \mathbb{R}^{d+1}$, and can perform integration over S^d.

5. Presence of two phases

In this section we show that, for the Lie group invariant Qs given in Sect. 4, the system defined by the partition function in Eq. (10) has two phases characterized by the topology of the distribution of $|\phi^j|^2$. The histograms of the distributions for $Q^{SO(2)}$, $Q^{SO(3)}$, and $Q^{SO(4)}$ are shown in Figs. 2, 3, and 4, respectively. Here we often take $\alpha = 0.5$ from Sect. 4, because the classical phase is most evident in the range $0 \lesssim \alpha \lesssim 1$, as will be explained more in Sect. 9. As can be seen

Downloaded from https://academic.oup.com/ptep/article/2022/4/043A01/6547023 by Kyoto Daigaku Nogaku-bu Toshoshitsu user on 23 January 2023

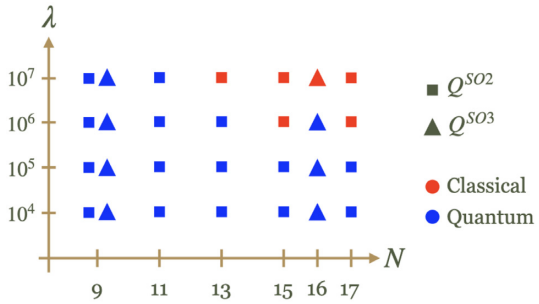

Fig. 5. The values of λ, N are classified according to the phases for $Q^{SO(2)}$ and $Q^{SO(3)}$ with $\alpha = 0.5$. The classification here is qualitative and contains some ambiguities, since it is based on the appearance of the histograms and not on a quantitative measure.

in the histograms, the two phases can be characterized by the number of connected regions of the distributions, one for smaller λ and two for larger λ. An important property of the latter phase is that the widths of each bunch of distributions are smaller than in the former. Because of this suppression of the fluctuations, we call the former and the latter phases the quantum and the classical phases, respectively, as we will see more evidence of the classical nature of the latter phase. We also call the two bunches of distributions in the classical phase the center and the outer bunches based on their distances from the origin.

Figure 5 classifies the values of λ and N according to the phases. In general, the classical phase appears when λ and N are large. Note that this classification is merely qualitative, as it is based on the appearance of the histograms, not on a quantitative measure. A possible quantitative measure could be given by the method developed in Ref. [46]. Applications of such measures to our setup are left for future study.

The transition resembles a matrix model counterpart, namely the transition between the one-cut and the two-cut solutions of the matrix model in the large-N limit [24], or the Gross–Witten–Wadia-type transition [25,26]. However, there is a difference in the mechanism of the distribution between our setup and the matrix model. When λ is large, the partition function in Eq. (10) approximately imposes the relation

$$Q_{abc} = \sum_{j=1}^{R} \phi_a^j \phi_b^j \phi_c^j. \tag{24}$$

This is a decomposition of a tensor Q into a number of vectors ϕ^j, and is known as the tensor rank decomposition (also often called CP decomposition) [47,48] in applied mathematics [49]. It is used for various purposes to extract information from tensors constructed from real-life data [50]. Tensor rank decomposition can also be used to extract geometric information from tensors [43]. The minimum value of R which realizes the decomposition in Eq. (24) for a given Q is called the rank[8] of Q. The ranks of the Qs in the cases of Figs. 2, 3, and 4 are smaller than the values of R in Eq. (5).[9] This generally means that there exist continuously infinite numbers of solutions of ϕ for Eq. (24), and they appear as the distributions in the figures. On the other

[8] More precisely, in the current case of real symmetric Q and the real symmetric form of each summand on the right-hand side of Eq. (24), the rank is called the real symmetric rank of Q.

[9] The ranks of the Qs in the cases of Figs. 2, 3, and 4 can be estimated as 22, 32, and 82, respectively. These are obtained by counting the numbers of the ϕ^j in the outer bunches and can also be checked by numerically performing the tensor rank decomposition by the program previously used in Ref. [43].

Downloaded from https://academic.oup.com/ptep/article/2022/4/043A01/6547023 by Kyoto Daigaku Nogaku-bu Toshoshitsu user on 23 January 2023

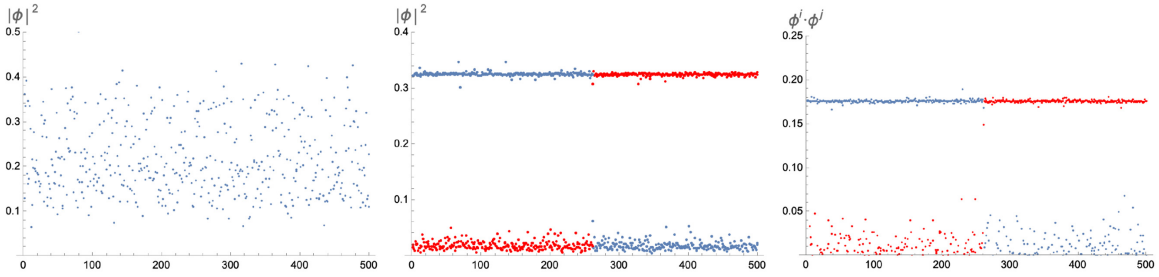

Fig. 6. Left: The Monte Carlo sequence of one of the $|\phi^j|^2$s for $Q^{SO(2)}$ with $N = 15$ ($\Lambda = 7$), $\lambda = 10^4$, and $\alpha = 0.5$. The vertical axis represents $|\phi^j|^2$ and the horizontal the sequence. The fluctuation of $|\phi^j|^2$ is wide. Middle: Two $|\phi^j|^2$s are plotted for $\lambda = 10^7$, one in the center bunch and the other in the outer bunch. The fluctuations around each center are strongly suppressed. However, an exchange occurs where one, say ϕ^1 colored blue, moves from the outer bunch to the center, while the other, say ϕ^2 colored red, moves in the opposite direction at the same time. They inherit each other's role. Right: At the exchange $\phi^1 \leftrightarrow \phi^2$, the inner products, $\phi^1_a \phi^3_a$ and $\phi^2_a \phi^3_a$, are exchanged, where ϕ^3 is in the outer bunch, but there are no net changes of the set of values.

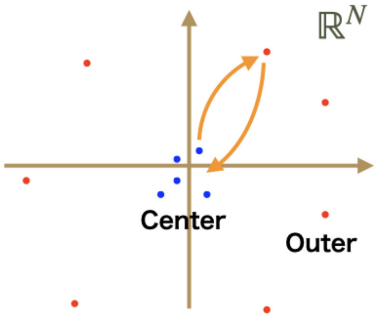

Fig. 7. Illustration of an exchange of ϕ^js between the center and the outer bunches. Such exchanges do not occur (or seem to be strongly suppressed) between ϕ^js in the outer bunch. As λ becomes larger, the exchanges are more suppressed.

hand, in the matrix model the eigenvalue distribution comes from the distribution of the matrix itself, while the tensor Q is an external parameter in our setup.

It is interesting to look at the actual Monte Carlo sequences. Figure 6 shows a few examples of the sequences of $|\phi^j|^2$ and $\phi^i_a \phi^j_a$ $(i \neq j)$ in the two phases. The left panel corresponds to the quantum phase, and the middle and the right panels the classical. In the quantum phase, $|\phi^j|^2$ fluctuates over a wider region. On the other hand, in the classical phase the fluctuations are confined around the centers of the two bunches, being strongly suppressed in the examples (how strongly depends on each case). Interestingly, as shown in the middle and right panels, we still observe exchanges of ϕ^j between the two bunches in our Monte Carlo sequences: one ϕ^j in the center bunch moves into the outer bunch, and at the same time one in the outer bunch moves into the center bunch (see Fig. 7 for an illustration). However, the exchange is just a replacement of the roles: there are no net changes of the values of $|\phi^j|^2$ and $\phi^i_a \phi^j_a$ as a whole in the outer bunch. Such an exchange does not seem to occur (or is strongly suppressed) between ϕ^js in the outer bunch. We also observe that, as the parameter λ becomes larger, the exchanges of any of these kinds are more suppressed, and the separation between the center and outer bunches becomes more strict.

Downloaded from https://academic.oup.com/ptep/article/2022/4/043A01/6547023 by Kyoto Daigaku Nogaku-bu Toshoshitsu user on 23 January 2023

This observation suggests the following picture of the classical phase. Suppose that it has been confirmed that the distributions, namely the center and outer bunches, are completely separated in a certain thermodynamic limit, as in the two-cut solutions of the matrix model in the large-N limit. More explicitly, the tensor rank decomposition in Eq. (24) splits into two parts,

$$Q_{abc} = \sum_{\phi^j \in \{\text{outer}\}} \phi^j_a \phi^j_b \phi^j_c + \sum_{\phi^j \in \{\text{center}\}} \phi^j_a \phi^j_b \phi^j_c, \tag{25}$$

where the first part actually dominates,

$$Q_{abc} \sim \sum_{\phi^j \in \{\text{outer}\}} \phi^j_a \phi^j_b \phi^j_c, \tag{26}$$

since $\phi^j \sim 0$ for $\phi^j \in \{\text{center}\}$. It turns out that, in our examples, the decomposition in Eq. (26) is actually the one with the minimum number of vectors: the tensor rank decomposition of Q with the rank of Q is dynamically performed. This should be taken as a surprise, because obtaining the rank of a tensor is known to be NP-hard [51]. In other words, the dynamics of the system solves this hard problem.

Since, as mentioned above, the ϕ^j in the outer bunch will not be exchanged with each other in such a thermodynamic limit,

$$\left\{\phi^i_a \phi^j_a \mid \forall \phi^i, \phi^j \in \text{Outer bunch}\right\} \tag{27}$$

will provide a set of semi-classical order parameters characterizing the classical phase. The inner products $\phi^i_a \phi^j_a$ are called overlaps and are used for order parameters in the replica method in the spin-glass theory [52]. Since the splitting of the center and outer bunches of the ϕ^j and the pattern in Eq. (27) generally breaks the replica symmetry, the transition to the classical phase can be regarded as a replica symmetry breaking. In Sect. 7 we associate the pattern of the set of order parameters in Eq. (27) with classical geometric structure of emergent spaces.

6. Tensor rank decomposition and geometry

6.1. *Integral representation of Q*

In CTM, the dynamical variable Q_{abc} is interpreted as a data set representing the geometry of a Cauchy hypersurface Σ. A procedure to obtain Q corresponding to a given d-dimensional compact Riemannian manifold (Σ, γ) was given in Ref. [43]. What is done in Sect. 4 can be regarded as some special cases of the general procedure. This is briefly summarized below.

1. Let i run from 1 to d, and let (x^i) be the local coordinate on Σ. The Laplace–Beltrami operator Δ is defined by
$$\Delta = \frac{1}{\sqrt{\gamma}} \partial_i \left(\sqrt{\gamma} \gamma^{ij} \partial_j\right)$$
from the metric tensor γ_{ij} on Σ and its determinant $\gamma = \det(\gamma_{ij})$.
2. Since Σ is a compact manifold, $-\Delta$ on Σ has a discrete spectrum, and we take N of its eigenvalues, starting with the smallest, and index them so that $0 \leq e_1 \leq \cdots \leq e_N$ is satisfied. Furthermore, let f_a be the eigenfunction belonging to the eigenvalue e_a and be orthonormalized like
$$\delta_{ab} = \int_\Sigma f_a(x) f_b(x) \sqrt{\gamma} d^d x. \tag{28}$$

Downloaded from https://academic.oup.com/ptep/article/2022/4/043A01/6547023 by Kyoto Daigaku Nogaku-bu Toshoshitsu user on 23 January 2023

When Σ is a closed manifold, or when it has boundaries with the Neumann boundary condition on f_a, the smallest eigenvalue e_1 is zero and $f_1(x)$ is a constant function. By the normalization condition, $f_1(x)$ is given by $V^{-1/2}$, where V is the volume, $V = \int_\Sigma \sqrt{\gamma} d^d x$.

3. The eigenfunctions $\tilde{f}_a$ with a damping factor are defined by $e^{-\alpha e_a} f_a(x)$, and

$$\begin{aligned} Q_{abc}(\alpha) &= A \int_\Sigma \tilde{f}_a(x)\tilde{f}_b(x)\tilde{f}_c(x)\sqrt{\gamma}d^d x \\ &= A e^{-\alpha(e_a+e_b+e_c)} \int_\Sigma f_a(x) f_b(x) f_c(x)\sqrt{\gamma}d^d x. \end{aligned}$$

The real constant A can be taken freely, but in this section we assume $A = 1$.

Since the constancy of f_1 is very useful in the analysis, in the following discussion we consider the case where (Σ, γ) is either a closed manifold or has boundaries with the Neumann boundary condition on f_a. Note also that $e_1 = 0$ follows in such cases.

6.2. *Discretization of integration*

In this subsection we consider discretizing the integration on Σ and its expression by summation. Let us consider a set $\{p_i \in \Sigma \mid i = 1, 2, \ldots, R\}$ of R points which are more or less uniformly distributed on Σ. The Voronoi cell of p_i is defined by

$$\sigma_i = \{p \in \Sigma \mid \ell(p, p_i) \le \ell(p, p_j) \text{ for all } j\},$$

where $\ell(p, q)$ is the geodesic distance between p and q. By this definition, the points equidistant from p_i and p_j are included in both σ_i and σ_j. Since $\bigcup_i \sigma_i = \Sigma$ holds, the full volume V of Σ is the sum of the volumes V_i of the σ_i. With the preparations above, we consider the integration of a scalar function $\phi(x)$ over Σ. We assume that $\phi(x)$ does not fluctuate violently and that the Voronoi cells are sufficiently small (i.e. R is large). Then the integration can be asymptotically approximated by

$$\int_\Sigma \phi(x)\sqrt{\gamma}d^d x = \sum_{i=1}^R \int_{\sigma_i} \phi(x)\sqrt{\gamma}d^d x \simeq \sum_{i=1}^R \phi(p_i) \int_{\sigma_i} \sqrt{\gamma}d^d x = \sum_{i=1}^R \phi(p_i) V_i,$$

where the average value of $\phi(x)$ on σ_i has been approximated by $\phi(p_i)$, the value at a representative point p_i. This approximation transforms the integration into the summation and vice versa.

6.3. *Tensor rank decomposition and Laplacian*

As discussed in Sect. 6.1, the tensor Q is defined by the integration over a Cauchy hypersurface Σ. By using the discussion in Ref. 6.2, Q can be approximated by a sum,

$$Q_{abc} = \int_\Sigma \tilde{f}_a(x)\tilde{f}_b(x)\tilde{f}_c(x)\sqrt{\gamma}d^d x \simeq \sum_{i=1}^R \tilde{f}_a(p_i)\tilde{f}_b(p_i)\tilde{f}_c(p_i)V_i.$$

Then, by defining $\phi^i_a = \tilde{f}_a(p_i)V_i^{1/3}$, we get an expression which has the form of the tensor rank decomposition:

$$Q_{abc} \simeq \sum_{i=1}^R \phi^i_a \phi^i_b \phi^i_c. \tag{29}$$

This means that the discretization of the integral representation of Q corresponds to the tensor rank decomposition of Q.

Downloaded from https://academic.oup.com/ptep/article/2022/4/043A01/6547023 by Kyoto Daigaku Nogaku-bu Toshoshitsu user on 23 January 2023

Finally, we explain the method for getting the geometric information from ϕ^i_a. Let us define $K^{ij} = \phi^i_a \phi^j_a$. The following approximation shows that this quantity is related to the "fuzzy" heat kernel $Z_N(p, q; \alpha)$:

$$K^{ij} = \tilde{f}_a(p_i)\tilde{f}_a(p_j)V_i^{1/3}V_j^{1/3} = \sum_{a=1}^{N} e^{-2\alpha e_a} f_a(p_i) f_a(p_j) V_i^{1/3} V_j^{1/3}$$
$$= Z_N(p_i, p_j; 2\alpha) V_i^{1/3} V_j^{1/3}, \tag{30}$$

where $Z_N(p, q; \alpha)$ is defined by

$$Z_N(p, q; \alpha) = \sum_{a=1}^{N} e^{-\alpha e_a} f_a(p) f_a(q). \tag{31}$$

The limit $N \to \infty$ of $Z_N(p, q; \alpha)$ agrees with the standard heat kernel. We note that Z_N satisfies the heat equation

$$\frac{\partial}{\partial \alpha} Z_N(x, y; \alpha) = \Delta_x Z_N(x, y; \alpha).$$

From the normalization in Eq. (28), the eigenvalues of $Z_N(p, q; \alpha)$ are given by $e^{-\alpha e_a}$ ($a = 1, 2, \ldots, N$), and therefore solving the eigenproblem of $Z_N(p, q; \alpha)$ essentially determines the Laplacian (see Sect. 7.2 for details). This can be approximated by solving the eigenproblem of $Z_N(p_i, p_j; \alpha)$. Therefore, the result in Eq. (30) implies that the Laplacian can be determined from K^{ij}, if we determine V_i.

So, the next question is how V_i can be calculated. To answer this, let us first consider

$$\sum_{j=1}^{R} K^{ij} V_j^{2/3} = \sum_{a=1}^{N} e^{-2\alpha e_a} f_a(p_i) V_i^{1/3} \sum_{j=1}^{R} f_a(p_j) V_j$$
$$\simeq \sum_{a=1}^{N} e^{-2\alpha e_a} f_a(p_i) V_i^{1/3} \int_{\Sigma} f_a(x) \sqrt{\gamma} d^d x$$
$$= \sum_{a=1}^{N} e^{-2\alpha e_a} f_a(p_i) V_i^{1/3} \delta_{a,1} V^{1/2} = V_i^{1/3}.$$

This means that V_i can be identified as one of the solutions of

$$\sum_{j=1}^{R} K^{ij} X_j^{2/3} = X_i^{1/3}, \tag{32}$$

with all $X_i \geq 0$. At this stage, since Eq. (32) has been derived with approximations, it is not clear whether Eq. (32) always has a solution for a given ϕ^i_a, or, if so, whether a solution can be uniquely identified with V_i. These questions will be discussed in the following subsection.

6.4. *Tensor eigensystems*

The tensor eigenvector $(v_a) \in \mathbb{C}^N \setminus \{0\}$ and the associated eigenvalue $e \in \mathbb{C}$ of a symmetric tensor Q_{abc} are defined by [53–55]

$$Q_{abc} v_b v_c = e\, v_a. \tag{33}$$

If (v, e) is an eigensystem, its scaled pair (tv, te) with any $t \in \mathbb{C} \setminus \{0\}$ is also an eigensystem. This property introduces the natural identification $(v, e) \sim (tv, te)$. The total number of complex eigenvectors of Eq. (33) under this equivalence class has been shown to be $2^N - 1$, if it is finite [55].

Downloaded from https://academic.oup.com/ptep/article/2022/4/043A01/6547023 by Kyoto Daigaku Nogaku-bu Toshoshitsu user on 23 January 2023

We are interested in real solutions for real Q. Let us first point out that there always exists at least one real solution. The proof is as follows. Unless $Q = 0$, $Q_{abc}v_a v_b v_c$ has a maximum positive value on the sphere $|v| = 1$. By applying the method of the Lagrange multiplier, the equation for the maximum leads to the same equation as Eq. (33), where $e > 0$ for a positive maximal value.

Now, to discuss the relation between Eqs. (33) and (32), let us consider a solution of Eq. (33) with $e \neq 0$. One can always take $(v, e) \sim (v', 1)$ by taking $t = 1/e$, and can put Eq. (33) into the form

$$Q_{abc}v_b v_c = v_a. \tag{34}$$

By putting the tensor rank decomposed form of the tensor Q in Eq. (29) into Eq. (34), we obtain

$$\sum_{j=1}^{R} \phi_a^j (v^j)^2 = v_a, \tag{35}$$

where $v^j = \phi_a^j v_a$. By multiplying both sides of Eq. (35) by ϕ_a^i and taking the contraction, we get

$$\sum_{j=1}^{R} K^{ij} (v^j)^2 = v^i. \tag{36}$$

If all the $v^i \geq 0$, one can obtain the solution to Eq. (32) by identifying $X_i = (v^i)^3$. In other words, there are as many solutions to Eq. (32) as eigenvectors of Q satisfying ${}^\forall v^i \geq 0$.

It does not seem to be an easy problem to find the general conditions under which we can find the eigenvectors satisfying ${}^\forall v^i \geq 0$ and can uniquely identify V_i. Therefore, we restrict ourselves to just explicitly showing that, when R is large enough and α is large enough, the eigensystem equation in Eq. (34) has a solution $X_i \simeq V_i$.

From $\tilde{f}_1(x) = V^{-1/2}$ and $e_1 = 0$, we get a formula for Q_{1ab}:

$$Q_{1ab} = e^{-\alpha(e_a+e_b)} V^{-1/2} \int_\Sigma f_a(x) f_b(x) \sqrt{\gamma} d^d x = V^{-1/2} e^{-2\alpha e_a} \delta_{ab}. \tag{37}$$

By using this, we can find

$$Q_{1ab} v_a v_b = V^{-1/2} \sum_{a\geq 1} e^{-2\alpha e_a} v_a^2 = V^{-1/2} v_1^2 + V^{-1/2} \sum_{a\geq 2} e^{-2\alpha e_a} v_a^2.$$

Therefore, by using Eq. (34), the $a = 1$ component of Eq. (34) can be rewritten as

$$\sum_{a\geq 2} e^{-2\alpha e_a} v_a^2 = v_1 (V^{1/2} - v_1). \tag{38}$$

For any real vector v_a, the left-hand side of Eq. (38) cannot be negative. This implies $0 \leq v_1 \leq V^{1/2}$, and in particular, if $v_1 = 0$ or $v_1 = V^{1/2}$, we have $v_a = 0$ for all $a \geq 2$. In fact, $(v_a) = (V^{1/2}, 0, 0, \ldots)$ is a solution to Eq. (34), because

$$Q_{abc}v_b v_c = Q_{a11} v_1 v_1 = 0 \qquad (\text{for } a \geq 2), \tag{39}$$

from Eq. (37). We note that the inner product of $\tilde{f}_a(x)$ and the non-zero solution $(v_a) = (V^{1/2}, 0, 0, \ldots)$ is equal to 1. Correspondingly, $v^i = \phi_a^i v_a \simeq V_i^{1/3} \tilde{f}_a(p_i) v_a = V_i^{1/3}$, meaning $X_i \simeq V_i$. This implies that, if R is sufficiently large, there will always be such a solution to Eq. (36).

Downloaded from https://academic.oup.com/ptep/article/2022/4/043A01/6547023 by Kyoto Daigaku Nogaku-bu Toshoshitsu user on 23 January 2023

Furthermore, if we also assume $\alpha \gg 1/e_2$, any eigenvector of Q gives $X_i \simeq V_i$. This can be shown in the following way. First of all, we know that

$$Q_{abc}v_bv_c = 2Q_{ab1}v_bv_1 + \sum_{b,c\geq 2} Q_{abc}v_bv_c = 2V^{-1/2}e^{-2\alpha e_a}v_av_1 + \sum_{b,c\geq 2} Q_{abc}v_bv_c$$

for $a \geq 2$. So the $a \geq 2$ components of Eq. (34) can be rewritten as

$$\sum_{b,c\geq 2} Q_{abc}v_bv_c = v_a(1 - 2V^{-1/2}e^{-2\alpha e_a}v_1). \tag{40}$$

Since the right-hand side of Eq. (38) is less than or equal to $V/4$, we can see that $|v_a| \leq e^{\alpha e_a}V^{1/2}/2$ for all $a \geq 2$. Based on this, the absolute value of the left-hand side of Eq. (40) can be bounded from above in the following way:

$$\begin{aligned}\left|\sum_{b,c\geq 2} Q_{abc}v_bv_c\right| &= \left|\sum_{b,c\geq 2} Q^{(\alpha=0)}_{abc}e^{-\alpha(e_a+e_b+e_c)}v_bv_c\right| \\ &\leq e^{-\alpha e_a}\sum_{b,c\geq 2}\left|Q^{(\alpha=0)}_{abc}\right|\left|e^{-\alpha e_b}v_b\right|\left|e^{-\alpha e_c}v_c\right| \\ &\leq e^{-\alpha e_a}\sum_{b,c\geq 2}\frac{V}{4}\left|Q^{(\alpha=0)}_{abc}\right|.\end{aligned}$$

Clearly, this asymptotically approaches zero for $\alpha \gg 1/e_2$. On the other hand, the absolute value of the right-hand side of Eq. (40) is asymptotically equal to $|v_a|$. Combining the above results, we find that v_a approaches zero for all $a \geq 2$ and, by Eq. (38), v_1 must be equal to $V^{1/2}$. This means that the solution approaches the above solution $(v_a) = (V^{1/2}, 0, 0, \ldots)$ or it is the above solution itself. By the same argument as above, the solution gives $v^i \simeq V_i^{1/3}$, meaning $X_i \simeq V_i$.

7. Geometric properties of the outer bunch

In this section we show that, in the classical phase, the pattern of the set of order parameters in Eq. (27) forms an object which has the geometry expected from the Lie group invariance of Q. We will demonstrate this for the Qs constructed in Sect. 4.

7.1. *Topology*

Let us first consider $Q^{SO(2)}$. As shown in Sect. 5, the inner products $\phi^i_a\phi^j_a$ within the outer bunch almost take constant values in a Monte Carlo sequence in the classical phase. Therefore, we do not lose generality by picking up one arbitrary sample of ϕ from a Monte Carlo sequence as a representative. Then we take all the ϕ^i in the outer bunch, based on their sizes $(\phi^i)^2$ separating them from those in the center bunch. For the case in Fig. 8, the number of ϕ^i in the outer bunch is 22 out of the total number $R = 76$ (namely, the replica number in Eq. (5) for $N = 15$). Then, as shown in the left panel of Fig. 8, we compute all the mutual distances between the ϕ^i in the outer bunch, identify the nearest neighbor pairs of ϕ^i, and connect them with lines. After the process we find a lattice S^1, as in the right panel.

This can be done for $Q^{SO(3)}$ as well, and we find a lattice S^2 as in Fig. 9. The same thing can also be done for $Q^{SO(4)}$, but the corresponding figure is not shown, since it is difficult to see the topology of S^3 on a two-dimensional sheet.

Downloaded from https://academic.oup.com/ptep/article/2022/4/043A01/6547023 by Kyoto Daigaku Nogaku-bu Toshoshitsu user on 23 January 2023

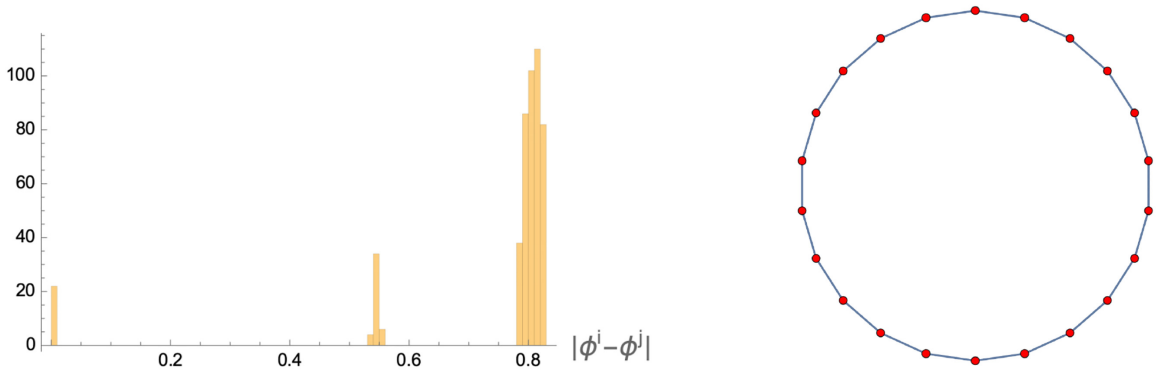

Fig. 8. Left: Histogram of the distances between all the pairs of ϕ^j in the outer bunch. The leftmost peak represents zero distance between ϕ^j themselves, and the peak around 0.55 represents the distances between the nearest neighbors. The parameters are $N = 15$ ($\Lambda = 7$), $\lambda = 10^7$, and $\alpha = 0.5$. Right: The nearest neighbor pairs of ϕ^j, which can be read from the bunch around 0.55 in the left histogram, are connected. In the figure, points represent each ϕ^j. Then, its topology is S^1.

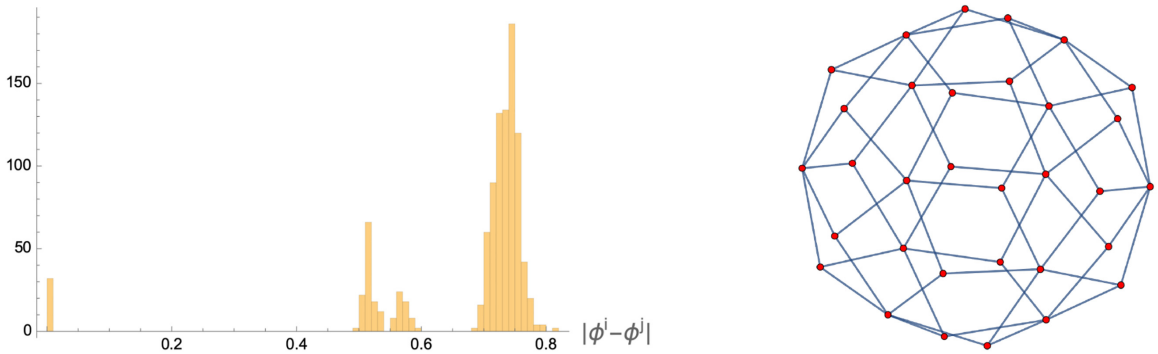

Fig. 9. Left: Histogram made as in Fig. 8 for $Q^{SO(3)}$ with $N = 16$ ($\Lambda = 3$), $\lambda = 10^7$, and $\alpha = 0.5$. Right: The nearest neighbor pairs of ϕ^js, which can be read from the bunch around 0.52 in the left histogram, are connected. Then, its topology is S^2.

7.2. *Spectra of Laplacian: Geometry*

An efficient way of detecting the geometry of an emergent space is to define a Laplacian on it and study the spectra. We will give two definitions and apply them to the configurations of the outer bunches obtained for $Q^{SO(n+1)}$. In both cases we obtain spectra consistent with the Laplacian on S^n, supporting the topological study in Sect. 7.1.

The first definition comes from Sect. 6. Since the construction of $Q^{SO(n+1)}$ is based on the method described there, it would be reasonable to employ the spectra of the Laplacian derived from the discussions there. The quantity defined in Eq. (31) can be regarded as an operator with eigenvalues $e^{-2\alpha e_a}$, where the e_a are the spectra of a Laplacian, in the following sense:

$$\int_\Sigma d^d q\,\sqrt{\gamma}\,Z_N(p,q;2\alpha)f_b(q) = \int_\Sigma d^d q\sqrt{\gamma}\,\sum_{a=1}^{N} e^{-2\alpha e_a} f_a(p)f_a(q)f_b(q) = e^{-2\alpha e_b} f_b(p), \quad (41)$$

where we have used the orthonormal condition in Eq. (28). After discretization, this operation can be expressed by a matrix,

$$Z_N(p_i,p_j;2\alpha)V_j \simeq V_i^{-1/3} K^{ij} V_j^{2/3}, \quad (42)$$

Downloaded from https://academic.oup.com/ptep/article/2022/4/043A01/6547023 by Kyoto Daigaku Nogaku-bu Toshoshitsu user on 23 January 2023

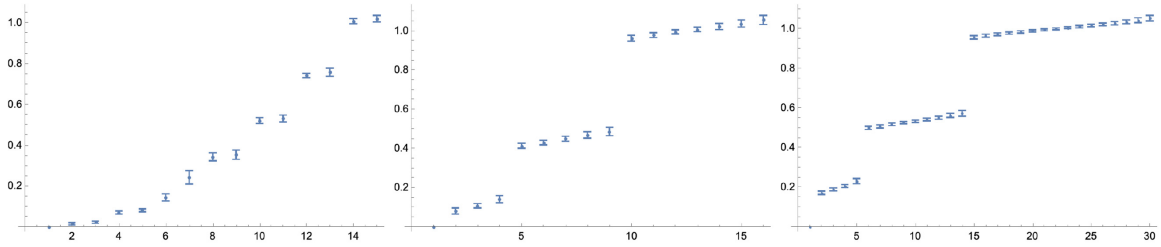

Fig. 10. The minus of the logarithm of the eigenvalues of L in Eq. (44) are plotted in order along the horizontal axis. The values are shifted vertically so that the smallest values are zero. $Q^{SO(n+1)}$ ($n = 1$, 2, 3) from left to right. The parameters are the same as in Figs. 2–4, with $\lambda = 10^{-7}$. $\tilde{R} = 22$, 32, and 82 respectively from left right. 500 samples from the sequences were statistically analyzed for each case.

where we have used Eq. (30). The expression on the right-hand side is inconvenient, because the matrix is not symmetric. By performing a similarity transformation by $V_i^{1/2}$ and $V_j^{-1/2}$ to Eq. (42) respectively from the left and the right, we obtain an equivalent eigenvalue problem with a symmetric matrix,

$$V_i^{1/6} K^{ij} V_j^{1/6}. \tag{43}$$

For convenience, let us relabel the ϕ^i in the outer bunch as ϕ^i ($i = 1, 2, \ldots, \tilde{R}$) without loss of generality, where $\tilde{R}$ is the total number of ϕ^j in the outer bunch. When $\tilde{R} > N$, which turns out to be our case, the matrix in Eq. (43) has at least $\tilde{R} - N$ zero eigenvalues, because Eq. (43) has the form of a product of two matrices, $(V_i^{1/6}\phi_a^i)(\phi_a^j V_j^{1/6})$, where the vector space associated with the lower index in the middle has the dimension N. Since we are only interested in the positive eigenvalues $e^{-2\alpha e_a}$, a convenient way to extract these positive eigenvalues is to consider the other way for the product of the two matrices,

$$L_{ab} := \sum_{i=1}^{\tilde{R}} \phi_a^i V_i^{1/6} V_i^{1/6} \phi_b^i = \sum_{i=1}^{\tilde{R}} \phi_a^i V_i^{1/3} \phi_b^i. \tag{44}$$

The eigenvalues of the matrix L give the spectra $e^{-2\alpha e_a}$. Here, the values of V_i are determined by solving Eq. (32).

We performed the above procedure for $Q^{SO(n+1)}$ ($n = 1$, 2, 3). In Fig. 10, the minus of the logarithm of the eigenvalues of L are plotted. The degeneracies and the values are consistent with what is expected for S^n. A curious matter is that the fifth and sixth eigenvalues in the S^1 case (the left panel) look deviated compared to the others. We have taken data from a few other Monte Carlo runs, but this seems to be universal for all the data of this S^1 case. This may imply an instability of S^1, but we do not currently have a good explanation.

Another definition of the Laplacian is to skip the procedure to determine V_i:

$$\tilde{L}_{ab} = \sum_{i=1}^{\tilde{R}} \phi_a^i \phi_b^i. \tag{45}$$

This definition more directly incorporates the replica symmetry of the system. Since this definition does not require positive solutions for V_i, it can be used for any circumstances, even in the quantum phase, where there would be quite a small chance of getting positive solutions for V_i. On the other hand, this definition relies on the assumption that the ϕ^i take reasonable values from the dynamics, while the former definition can absorb the ambiguities related to the discretization discussed in Sect. 6. We are not currently sure which one is better and must wait for future study, but we would expect that these two definitions would produce more or less

Downloaded from https://academic.oup.com/ptep/article/2022/4/043A01/6547023 by Kyoto Daigaku Nogaku-bu Toshoshitsu user on 23 January 2023

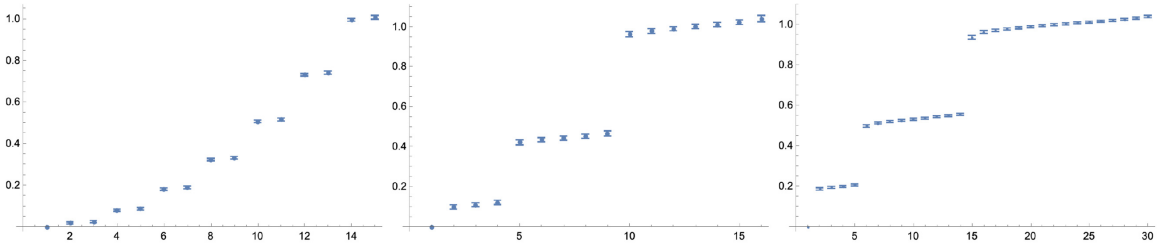

Fig. 11. As Fig. 10 for $\tilde{L}$ in Eq. (45).

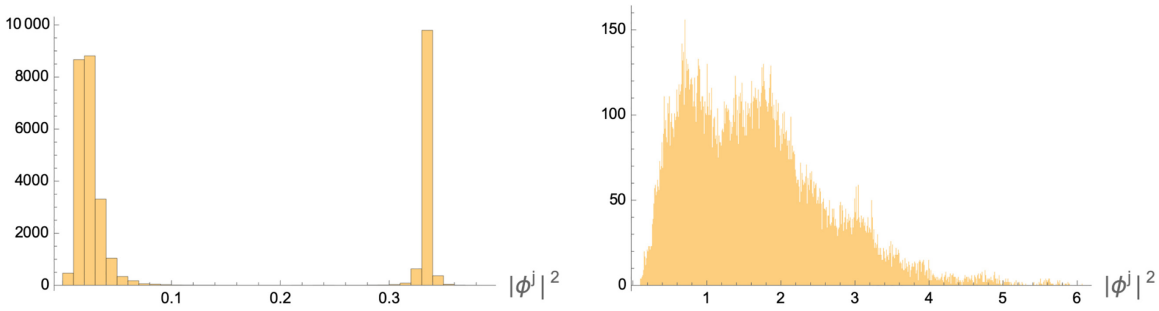

Fig. 12. Dependence of phases on representations. The examples are for $Q^{SO(2)}$ with $\Lambda = 7$, $\lambda = 10^7$, and $\alpha = 0.5$. Left: Histogram of $|\phi^j|^2$ when $p = 0$ is dropped. Right: $p = 0$, 1 are dropped.

identical results in the large-N limit in the classical phase. Figure 11 shows the spectra obtained from $\tilde{L}$, supporting the expectation.

8. Deformations of Q

In this section we study two kinds of deformations of Q from those given in Sect. 4.

8.1. *Dependence on representations*

In the construction of Lie group invariant Qs in Sect. 4, the vector spaces associated to the indices of Q are given by direct sums of some irreducible representation spaces of the Lie groups. The sets of irreducible representations considered there are taken successively from the trivial representation to the one indexed by a cut-off Λ. This is a natural choice from the physical point of view, since Λ can naturally be related to a short-distance cut-off in a space. In this section we consider some unnatural choices by dropping a few of the intermediate representations.

In Fig. 12 we consider $Q^{SO(2)}$ with $\Lambda = 7$, $\lambda = 10^7$, and $\alpha = 0.5$. As shown in Fig. 5, this case is in the classical phase, if we consider the full representations, $p = 0, 1, \ldots, \Lambda = 7$, namely $N = 15$. The left panel of Fig. 12 shows the histogram of $|\phi^j|^2$ when we drop the $p = 0$ representation. This is still in the classical phase. However, when we drop $p = 0, 1$, the phase becomes quantum, as shown in the right panel. In Fig. 13 we consider $Q^{SO(3)}$. Even dropping $l = 0$ changes the phase to quantum.

One would suspect that the change to the quantum phase is merely caused by the reduction of N due to dropping. However, dropping $p = 0, 1$ for $Q^{SO(2)}$ above corresponds to $N = 12$. According to Fig. 5, the case with $N = 12$ and $\lambda = 10^7$ is in between the quantum and classical phases, but the histogram on the right of Fig. 12 shows the clear characteristic of the quantum phase. Therefore, we see that dropping intermediate representations makes the classical phase

Downloaded from https://academic.oup.com/ptep/article/2022/4/043A01/6547023 by Kyoto Daigaku Nogaku-bu Toshoshitsu user on 23 January 2023

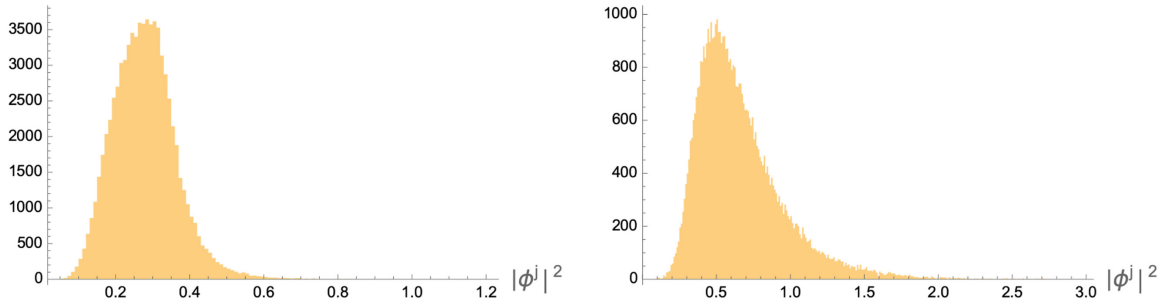

Fig. 13. Dependence of phases on representations. The examples are for $Q^{SO(3)}$ with $\Lambda = 3$, $\lambda = 10^7$, and $\alpha = 0.5$. Left: $l = 0$ is dropped. Right: $l = 0$, 1 are dropped.

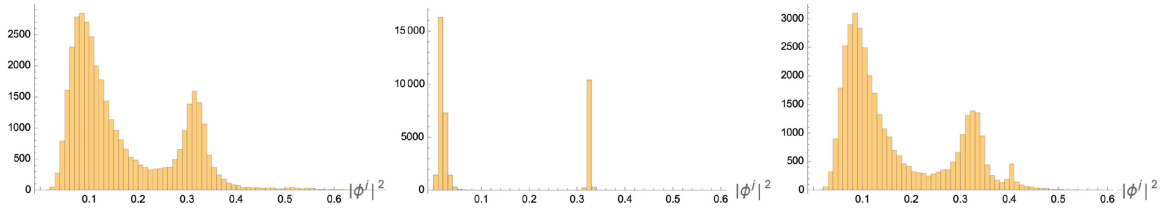

Fig. 14. Histograms of $|\phi^j|^2$ for $z = -24/85$, 0, 24/85 from left to right, respectively. The setting is $Q^{SO(2)}$ with $N = 15$ ($\Lambda = 7$), $\lambda = 10^7$, and $\alpha = 0.5$.

less likely. It is interesting that the most physically natural set of representations, i.e. successively taken from the trivial representation to a cut-off, makes the classical phase most likely.

8.2. *Breaking the Lie group invariance of Q*

In this subsection we break the Lie group invariance of Q by

$$Q = (Q^{SO(n)} + z\, Q^B)/\sqrt{1+z^2}, \tag{46}$$

where z is a deformation parameter, $Q^{SO(n)}$ is given in Sect. 4, and Q^B ($|Q_B| = 1$) is a tensor which breaks the Lie group invariance.

There are many possible such Q^Bs, and it is not feasible to study all of them. We therefore consider merely one such Q^B, which seems meaningless enough to consider it as reflecting the general effect. One way to give Q^B is to assign random values, but this would have the problem of reproducing the result. So, we rather consider a meaningless function to generate Q^B. More precisely, we consider

$$Q^B_{abc} = \text{const.} \times \begin{cases} \cos\left[0.1(a+b+c)\right] & \text{if } Q^{SO(n)}_{abc} = 0, \\ 0 & \text{otherwise,} \end{cases} \tag{47}$$

with the normalization const. for $|Q^B| = 1$. This also satisfies the transversality, $Q^{SO(n)}_{abc} Q^B_{abc} = 0$.

The result is shown in Fig. 14 for $Q^{SO(2)}$. Non-zero z makes the classical phase less likely.

We also observed a similar effect for $Q^{SO(3)}$ under the same perturbation, Eq. (47), which totally breaks the $SO(3)$ symmetry. We conclude that breaking Lie group invariance makes the classical phase less likely.

Downloaded from https://academic.oup.com/ptep/article/2022/4/043A01/6547023 by Kyoto Daigaku Nogaku-bu Toshoshitsu user on 23 January 2023

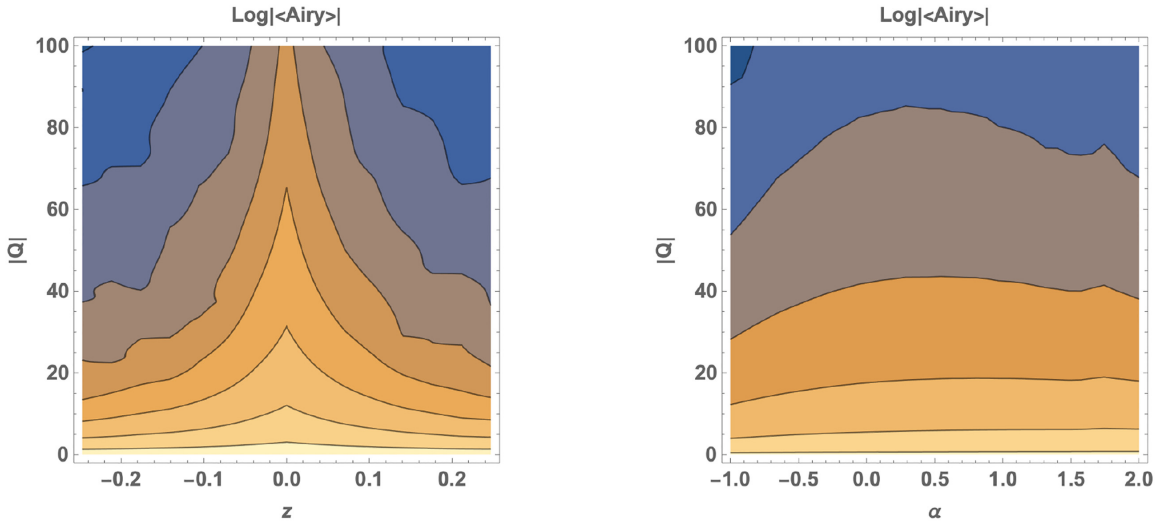

Fig. 15. Contour plots of $\log|\langle\prod \text{Airy}\rangle|$, the logarithm of the modulus of the expectation value. Left: A symmetry-breaking case from Sect. 8.2 with $Q^{SO(2)}$, $N = 15$ ($\Lambda = 7$), $\lambda = 10^7$, and $\alpha = 0.5$. The horizontal axis represents the breaking parameter z, and the vertical one $|Q|$. Right: An invariant case with $Q^{SO(2)}(\alpha)$; α varies along the horizontal axis. The other parameters are the same as in the left panel.

9. Behavior of the oscillatory part

In this section we discuss the oscillatory part,

$$\left\langle \prod_{i=1}^{R} \text{Airy}\left(-|Q|^{2/3}(\phi^i)^2\right)\right\rangle_{\tilde{Q},\lambda}, \tag{48}$$

in Eq. (11), where $\tilde{Q} = Q/|Q|$. Here note that we have dropped the dependence of the coupling parameter on $|Q|^2$ compared to Eq. (11). The reason for this simplification is that changing the coupling parameter requires repeating Monte Carlo simulations with different couplings, and it would not be feasible to obtain results for many $|Q|$s. On the other hand, Eq. (48) for different $|Q|$s can be computed by using the same sampling data of ϕ from the Monte Carlo simulation. At the end of this section we speculate on the effect of re-including the dependence on $|Q|^2$.

The fluctuations of $|\phi^i|^2$ are larger in the quantum phase than in the classical phase. Since the Airy function, Eq. (13), in Eq. (48) is an oscillatory function, larger fluctuations make the expectation values smaller, because there are more cancellations. Therefore, Eq. (48) generally takes smaller values in the quantum phase than in the classical phase. In particular, there are more cancellations as $|Q|$ becomes larger, because of the $|Q|$ dependence in the argument of Eq. (48).

Figure 15 shows the results for the expectation values from the Monte Carlo simulations. In the left panel, a symmetry-breaking case in Sect. 8.2 is studied. As can be seen in the figure, the expectation value is strongly peaked around $z = 0$. This can be understood by the fact that the classical phase around $z = 0$ is surrounded by the quantum phase, as shown in Sect. 8.2. In the right panel, the dependence of the expectation value on α is studied for $Q^{SO(2)}(\alpha)$. The expectation value depends moderately on α. As is shown in the histograms in Fig. 16, the system is in the classical phase throughout the region of α in the figure, but the widths of the bunches depend on α. The widths become smallest in the middle case. This explains why there is a mild peak around $\alpha \sim 0.4$ in the right panel of Fig. 15.

Downloaded from https://academic.oup.com/ptep/article/2022/4/043A01/6547023 by Kyoto Daigaku Nogaku-bu Toshoshitsu user on 23 January 2023

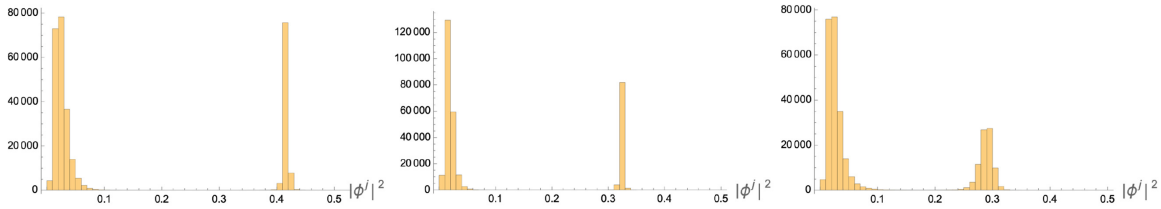

Fig. 16. Histograms of $|\phi^j|^2$ for $Q^{SO(2)}(\alpha)$ with $N = 15$ ($\Lambda = 7$), $\lambda = 10^7$, and $\alpha = -1$ (left), 19/35 (middle), and 2 (right).

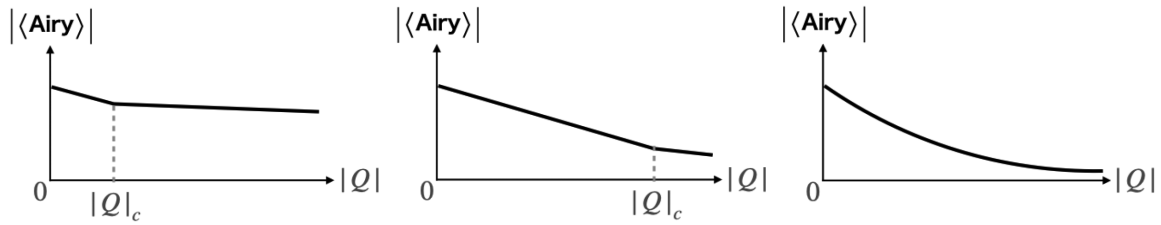

Fig. 17. Three possible behavior profiles of the expectation value. $|Q|_c$ denotes the transition point between the quantum phase ($|Q| < |Q|_c$) and the classical ($|Q| > |Q|_c$). $|Q|_c$ is smaller in the left panel than in the middle, where the former is expected for Lie group invariant $\tilde{Q}$ and the latter for non-invariant. It is even possible that there are no transitions at all, as in the right panel.

It is worth stressing here the importance of taking the cosmological constant of CTM to be positive in the discussions of this section. As explained in the last paragraph of Sect. 3, the Airy function part becomes oscillatory in the positive case, and the discussions above can be applied. On the other hand, when it is negative, the Airy function part becomes an exponentially damping function (see the last paragraph of Sect. 3) and the results will be different. In particular, we cannot expect the suppression of the configurations in the quantum phase discussed above, which will highlight those in the classical phase.

Lastly let us speculate on what happens when we reintroduce the dependence of the coupling on $|Q|^2$, i.e. $\lambda \to \lambda|Q|^2$ as in Eq. (11). Now $\lambda|Q|^2$ serves as an effective coupling. Then, the results from the previous sections tell us that when $|Q|$ is small the system is in the quantum phase. By increasing $|Q|$, the effective coupling becomes larger and the system will eventually undergo the transition to the classical phase at some value of $|Q|$, say $|Q|_c$, which generally depends on $\tilde{Q}$. Note, however, that there is also the possibility that there are no transitions to the classical phase at all for some $\tilde{Q}$. For Lie group invariant $\tilde{Q}$, $|Q|_c$ will be relatively smaller, while $|Q|_c$ will be larger for non-invariant $\tilde{Q}$. Since the expectation value decays more quickly in the quantum phase as $|Q|$ becomes larger, we would expect the three types of behavior shown in Fig. 17. In particular, larger expectation values are expected for Lie group invariant $\tilde{Q}$ in the large-$|Q|$ region.

10. Summary and future prospects

We have studied the wave function of the canonical tensor model [15] in the Q-representation, when the argument Q takes Lie group invariant or nearby values. Using the Monte Carlo method we found two phases, which we call the quantum and classical phases, where the fluctuations of the variables are suppressed in the latter phase relative to the former. In the classical phase, configurations emerge which are discretizations of classical geometric spaces invariant under the Lie group symmetries. More precisely, we demonstrated the emergence of configura-

Downloaded from https://academic.oup.com/ptep/article/2022/4/043A01/6547023 by Kyoto Daigaku Nogaku-bu Toshoshitsu user on 23 January 2023

tions corresponding to discretized S^n ($n = 1, 2, 3$) for $SO(n+1)$ invariant Q. The transition resembles a matrix model counterpart, namely the transition between the one-cut and the two-cut solutions in the matrix model [24], or the Gross–Witten–Wadia-type transition [25,26]. However, this resemblance is obscured by a difference: in our setup, the tensor is a given variable for each case and the distributions come from the abundance of tensor rank decompositions of the tensor, while in the matrix model, the matrix itself has distributions. We argue that complete splitting of the distributions in the classical phase will imply a replica symmetry breaking.

We also performed some preliminary studies on the phases and the transition. For larger N, the transition occurs for smaller λ, meaning that the classical phase is more favored for larger N. This implies that the emergence of classical spaces is more likely for larger N. We also presented some evidence for the importance of Lie group invariance and proper choices of representations for the appearance of the classical phase.

The main difference of the present work from Ref. [23] is the discovery of the classical phase. The previous work was not aware of the classical phase, and discussed only the quantum phase, and a fluid picture was argued to be useful for an approximate analytical treatment for Lie group invariant values of Q. On the other hand, in the classical phase found in this paper, the inner products $\phi^i_a \phi^j_a$ within the outer bunch take almost constant values with small fluctuations. This suggests that a more solid picture than a fluid is appropriate to describe the classical phase. In terms of this aspect, it would be an intriguing coincidence that the form of the real part $Z_{Q,\lambda}$ is similar to that of the p-spin spherical model for the spin glass [52,56]. This suggests that, recalling that the classical phase is accompanied with a replica symmetry breaking, the classical phase would actually be a glassy phase, meaning spacetime in CTM would have similarities with glass. It is an interesting future direction to pursue an approximate analytical method for the classical phase based on the picture obtained in this paper.

The results of this paper suggest the interesting possibility of applying CTM as a model for the evolution of the universe. As discussed in Sect. 9, the system is in the quantum phase when $|Q|$ is small, but will eventually undergo the transition to the classical phase when $|Q|$ grows and reaches a critical value depending on $Q/|Q|$, or it never will. This implies the scenario that the universe starts with the quantum phase with no definite geometry and then enters the classical phase with the emergence of a space with classical geometry, under the assumption that time is correlated with $|Q|$.[5] It would be a challenging and interesting direction of study to compute observable signals, such as primordial fluctuations, from the perspective of CTM, and check its significance by comparing with the actual observational data.

Another interesting direction for the application of CTM would be to consider more general values of Q than the Lie group invariant ones. The procedure developed in Sect. 6 to construct Q from geometric data can generally be applied to a wide range of curved geometries, such as ones with horizons, singularities, and so on. Putting these more general values of Q into the argument of the wave function and studying the properties of the system, such as its phase, would provide general ideas about how spacetime geometries are described in CTM. In particular, it would be worth studying black hole geometries from the perspective of CTM to shed new light on the long-standing paradox of information loss.

Many questions remain which must be answered in future studies. We have only studied the wave function for very particular values of the argument, namely Lie group invariant or nearby ones, but these particular choices cannot be well justified without a global view of the wave function profile. We have introduced the parameter λ for analytical convenience, but the removal

Downloaded from https://academic.oup.com/ptep/article/2022/4/043A01/6547023 by Kyoto Daigaku Nogaku-bu Toshoshitsu user on 23 January 2023

limit of taking it infinite has not been studied. We have computed $\langle \prod \mathrm{Airy} \rangle_{Q,\lambda}$ but not the Q dependence of $Z_{Q,\lambda}$, which is also needed to understand the whole profile of $\Psi(Q, \lambda)$. To answer these questions we would need analytical methods, rather than just relying on numerical computations. The pictures we have obtained so far provide hints toward them.

Last, but not least, the discovery of the classical phase of this paper suggests a new method of tensor rank decomposition [47,48]. Tensor rank decomposition is a useful method for extracting information from a tensor of real-life data [50], but there is no assurance of getting a good decomposition due to some fundamental problems, such as the ill-posedness [50] of the approximation problem and the difficulty [50,51] of computing the rank of a tensor. On the other hand, what happens in the classical phase is that, as in Eqs. (25) and (26), the ϕ^i are dynamically divided into two bunches, of which the outer bunch serves as a good approximation of the tensor rank decomposition of Q, while the center bunch is a small correction, which can be ignored practically. In other words, when we find a classical phase for a tensor Q by taking λ large, we can obtain an approximate tensor rank decomposition of Q. What seems interesting and useful here is that the rank, namely the number of ϕ^i in the outer bunch, is automatically determined by the dynamics of the Monte Carlo simulation, and we do not need to know the rank of Q in advance. This would be an advantage considering the difficulty of the rank determination, though the Monte Carlo simulation is costly. It would be interesting to clarify how useful this method is in practice for various cases of Q.

Acknowledgments

The work of N. S. is supported in part by JSPS KAKENHI Grant No. 19K03825.

Funding

Open Access funding: SCOAP[3].

Appendix A. A minimal explanation of CTM

This appendix gives a minimal explanation of the canonical tensor model (CTM) to understand the origin of the wave function discussed in this paper. A longer but still concise summary can be found in Ref. [21, Sect. 2] with slightly different normalizations.

The dynamical variables of CTM are a canonical conjugate pair of real symmetric three-index tensors, Q_{abc} and P_{abc} ($a, b, c = 1, 2, \ldots, N$). The quantized variables satisfy

$$[\hat{Q}_{abc}, \hat{P}_{def}] = i \sum_{\sigma} \delta_{a\sigma_d} \delta_{b\sigma_e} \delta_{c\sigma_f},$$
$$[\hat{Q}_{abc}, \hat{Q}_{def}] = [\hat{P}_{abc}, \hat{P}_{def}] = 0, \tag{A1}$$

where the sum is over all the permutations of d, e, f. The expressions of the constraints are given by [31]

$$\hat{H}_a = \frac{1}{2} \left(\hat{P}_{abc} \hat{P}_{bde} \hat{Q}_{cde} + 2iR \hat{P}_{abb} - \Lambda_c \hat{Q}_{abb} \right),$$
$$\hat{J}_{[ab]} = \frac{1}{4} \left(\hat{P}_{acd} \hat{Q}_{bcd} - \hat{P}_{bcd} \hat{Q}_{acd} \right), \tag{A2}$$

where the value of R is determined to be $R = (N + 2)(N + 3)/4$ by requiring the hermiticity of $\hat{H}_a$ [31]. The square bracket in $\hat{J}_{[ab]}$ is to represent the antisymmetry $\hat{J}_{[ab]} = -\hat{J}_{[ba]}$. Λ_c is a real parameter, which will be explained more below.

Downloaded from https://academic.oup.com/ptep/article/2022/4/043A01/6547023 by Kyoto Daigaku Nogaku-bu Toshoshitsu user on 23 January 2023

The commutation algebra among the above constraints is given by [31,33]

$$\begin{aligned}
[\hat{H}\xi^1, \hat{H}\xi^2] &= i\hat{J}([\hat{P}\xi^1, \hat{P}\xi^2] + 2\Lambda_c[\xi^1, \xi^2]),\\
[\hat{J}\eta, \hat{H}\xi] &= i\hat{H}(\eta\xi),\\
[\hat{J}\eta^1, \hat{J}\eta^2] &= i\hat{J}([\eta^1, \eta^2]),
\end{aligned} \tag{A3}$$

where we have introduced auxiliary c-number variables ξ_a, $\eta_{[ab]}$ and

$$\begin{aligned}
&\hat{H}\xi := \hat{H}_a\xi_a, \qquad \hat{J}\eta := \hat{J}_{[ab]}\eta_{[ab]}, \qquad (\hat{P}\xi)_{ab} := \hat{P}_{abc}\xi_c,\\
&[\xi^1, \xi^2]_{ab} := \xi^1_a\xi^2_b - \xi^1_b\xi^2_a, \qquad (\eta\xi)_a := \eta_{[ab]}\xi_b,
\end{aligned} \tag{A4}$$

to simplify the expressions. The algebraic structure in Eq. (A3) of the constraints resembles that of ADM [19], and in particular there exist variable-dependent structure coefficients on the right-hand side of the first line, which is also similar to ADM.

The physical state conditions are given by

$$\hat{H}_a|\Psi\rangle = \hat{J}_{[ab]}|\Psi\rangle = 0. \tag{A5}$$

A systematic solution to the above conditions valid for general N was found in Ref. [33], and is given by

$$\langle P|\Psi\rangle = \int_{\mathcal{C}} d\phi\, d\tilde{\phi}\, \exp\left[i\sum_{j=1}^{R}\left(P_{abc}\phi^j_a\phi^j_b\phi^j_c - \phi^j_a\phi^j_a\tilde{\phi}^j + \frac{4}{27\Lambda_c}(\tilde{\phi}^j)^3\right)\right] \tag{A6}$$

in the P-representation. This integral can be regarded as a holomorphic integration on an $(N+1)R$-dimensional curve $\mathcal{C}$, and the curve is supposed to be taken so that the integration is convergent. The choice of $\mathcal{C}$ can in principle be rigorously made explicit by applying Picard–Lefschetz theory [34].

It has been shown [30] that the $N = 1$ case of CTM is equivalent to the mini-superspace approximation of general relativity, where Λ_c corresponds to the cosmological constant. From this fact, Λ_c is called the cosmological constant of CTM in the text. The positivity of Λ_c is essential for the appearance of the peak Lie group relation [21,22] mentioned in Sect. 1. As can be checked in Eq. (A2) and the other equations, the size of Λ_c can be changed freely by performing $(Q, P) \to (xQ, P/x)$ with real x without changing the above commutation relations. This means that the size is physically irrelevant and there are only discrete choices, say $\Lambda_c = 0, \pm 1$. The expression of the wave function in Eq. (3) in the text corresponds to $\Lambda_c = 4/9$ in Eq. (A6), which is convenient because then the $\tilde{\phi}$ integration in the wave function can be related to the Airy function, Eq. (12), with no extra numerical coefficients.

Appendix B. Spherical harmonics on S^d

Let us take a spherical coordinate system $(\varphi, \theta_1, \ldots, \theta_{d-1})$ on S^d with $\varphi \in [-\pi, \pi)$, $\theta_i \in [0, \pi]$. If we write ds_d as the line element on S^d, ds^2_d can be determined inductively as follows:

$$\begin{aligned}
ds^2_1 &= d\varphi^2,\\
ds^2_{d+1} &= \sin^2\theta_d ds^2_d + d\theta^2_d.
\end{aligned}$$

Downloaded from https://academic.oup.com/ptep/article/2022/4/043A01/6547023 by Kyoto Daigaku Nogaku-bu Toshoshitsu user on 23 January 2023

By these relations, the Laplace–Beltrami operator Δ_d on S^d is also determined inductively as follows:

$$\Delta_1 = \frac{\partial^2}{\partial\varphi^2},$$
$$\Delta_{d+1} = \frac{1}{\sin^d\theta_d}\frac{\partial}{\partial\theta_d}\left(\sin^d\theta_d\frac{\partial}{\partial\theta_d}\right) + \frac{\Delta_d}{\sin^2\theta_d}.$$

The d-dimensional harmonic function on S^d is specified by an array of d integers $L_d = (m, l_1, \ldots, l_{d-1})$ with $|m| \le l_1 \le \cdots \le l_{d-1}$, and is written as $Y_{d;L_d}(\varphi, \theta_1, \ldots, \theta_{d-1})$. This satisfies the Helmholtz equation,

$$\Delta_d Y_{d;L_d} = -l_{d-1}(l_{d-1} + d - 1)Y_{d;L_d}.$$

If we assume $Y_{d+1;L_{d+1}}(\varphi, \theta_1, \ldots, \theta_d) = Y_{d;L_d}(\varphi, \theta_1, \ldots, \theta_{d-1})\,\Theta(\theta_d)$, $\Theta(\theta_d)$ must be a solution of the equation

$$\frac{1}{\sin^d\theta_d}\frac{d}{d\theta_d}\left(\sin^d\theta_d\frac{d\Theta}{d\theta_d}\right) - \frac{l_{d-1}(l_{d-1}+d-1)}{\sin^2\theta_d}\Theta = -l_d(l_d+d)\Theta. \tag{B1}$$

The non-singular solutions of Eq. (B1) can be written as [44]

$$\Theta(\theta_d) \propto \frac{1}{\sin^{(d-1)/2}\theta_d}P^{-(l_{d-1}+\frac{d-1}{2})}_{l_d+\frac{d-1}{2}}(\cos\theta_d) \propto \sin^{l_{d-1}}\theta_d\, C^{l_{d-1}+\frac{d}{2}}_{l_d-l_{d-1}}(\cos\theta_d),$$

where $P^\mu_\nu(x)$ is the Ferrers function (or Legendre function) of the first kind and $C^\lambda_n(x)$ is the Gegenbauer polynomial. They have the relation

$$C^\lambda_n(\cos\theta) = \frac{\sqrt{\pi}\,\Gamma(n+2\lambda)}{2^{\lambda-\frac{1}{2}}n!\Gamma(\lambda)}(\sin\theta)^{\frac{1}{2}-\lambda}P^{\frac{1}{2}-\lambda}_{n+\lambda-\frac{1}{2}}(\cos\theta). \tag{B2}$$

This result gives a way of defining the spherical harmonics inductively as follows:

$$Y_{d+1;L_{d+1}}(\varphi, \theta_1, \ldots, \theta_d) = A_{d+1;L_{d+1}}\sin^{l_{d-1}}\theta_d\, C^{l_{d-1}+\frac{d}{2}}_{l_d-l_{d-1}}(\cos\theta_d)\cdot Y_{d;L_d}(\varphi, \theta_1, \ldots, \theta_{d-1}),$$

with a normalization factor $A_{d+1;L_{d+1}}$. Since the Gegenbauer polynomials satisfy the orthogonality relation [57]

$$\int_{-1}^{1} C^\lambda_n(x)C^\lambda_m(x)(1-x^2)^{\lambda-\frac{1}{2}}dx = \int_0^\pi C^\lambda_n(\cos\theta)C^\lambda_m(\cos\theta)\sin^{2\lambda}\theta d\theta = \frac{2^{1-2\lambda}\pi\,\Gamma(n+2\lambda)}{(n+\lambda)\Gamma(\lambda)^2 n!}\delta_{n,m},$$

the orthogonality of $Y_{d+1;L_{d+1}}$ is also guaranteed. Furthermore, the normalization factor $A_{d+1;L_{d+1}}$ is determined by

$$\begin{aligned}
1 &= \int_{S^{d+1}} Y_{d+1;L_{d+1}}(\varphi, \theta_1, \ldots, \theta_d)^2 d^{d+1}\Omega \\
&= A^2_{d+1;L_{d+1}}\int_0^\pi C^{l_{d-1}+\frac{d}{2}}_{l_d-l_{d-1}}(\cos\theta_d)^2\sin^{2l_{d-1}+d}\theta_d d\theta_d \\
&= A^2_{d+1;L_{d+1}}\frac{2^{-(2l_{d-1}+d-1)}\pi(l_d+l_{d-1}+d-1)!}{\left(l_d+\frac{d}{2}\right)\Gamma\left(l_{d-1}+\frac{d}{2}\right)^2(l_d-l_{d-1})!}.
\end{aligned}$$

This shows the specific value of $A_{d+1;L_{d+1}}$:

$$A_{d+1;L_{d+1}} = \left(\frac{\left(l_d+\frac{d}{2}\right)\Gamma\left(l_{d-1}+\frac{d}{2}\right)^2(l_d-l_{d-1})!}{2^{-(2l_{d-1}+d-1)}\pi(l_d+l_{d-1}+d-1)!}\right)^{1/2}.$$

Collecting the results above, we obtain Eq. (19).

Downloaded from https://academic.oup.com/ptep/article/2022/4/043A01/6547023 by Kyoto Daigaku Nogaku-bu Toshoshitsu user on 23 January 2023

REFERENCES

[1] H. Georgi, Front. Phys. **54**, 1 (1999).
[2] M. Reuter and F. Saueressig, Quantum Gravity and the Functional Renormalization Group: The Road towards Asymptotic Safety (Cambridge University Press, Cambridge, 2019).
[3] A. Eichhorn, Front. Astron. Space Sci. **5**, 47 (2019) [arXiv:1810.07615 [hep-th]] [Search inSPIRE].
[4] R. Loll, Class. Quant. Grav. **37**, 013002 (2020) [arXiv:1905.08669 [hep-th]] [Search inSPIRE].
[5] C. Rovelli and F. Vidotto, Covariant Loop Quantum Gravity: An Elementary Introduction to Quantum Gravity and Spinfoam Theory (Cambridge University Press, Cambridge, 2014).
[6] S. Surya, Living Rev. Rel. **22**, 5 (2019) [arXiv:1903.11544 [gr-qc]] [Search inSPIRE].
[7] T. Konopka, F. Markopoulou, and L. Smolin, arXiv:hep-th/0611197 [Search inSPIRE].
[8] S. Wolfram, Complex Syst. **29**, 107 (2020) [arXiv:2004.08210 [cs.DM]] [Search inSPIRE].
[9] C. A. Trugenberger, J. High Energy Phys. **09**, 045 (2017) [arXiv:1610.05934 [hep-th]] [Search inSPIRE].
[10] P. Akara-Pipattana, T. Chotibut, and O. Evnin, J. Phys. A **54**, 425001 (2021) [arXiv:2102.11477 [cond-mat.dis-nn]] [Search inSPIRE].
[11] J. Ambjorn, B. Durhuus, and T. Jonsson, Mod. Phys. Lett. A **06**, 1133 (1991).
[12] N. Sasakura, Mod. Phys. Lett. A **06**, 2613 (1991).
[13] N. Godfrey and M. Gross, Phys. Rev. D **43**, R1749 (1991).
[14] R. Gurau, Commun. Math. Phys. **304**, 69 (2011) [arXiv:0907.2582 [hep-th]] [Search inSPIRE].
[15] N. Sasakura, Int. J. Mod. Phys. A **27**, 1250020 (2012) [arXiv:1111.2790 [hep-th]] [Search inSPIRE].
[16] V. Bonzom, R. Gurau, A. Riello, and V. Rivasseau, Nucl. Phys. B **853**, 174 (2011) [arXiv:1105.3122 [hep-th]] [Search inSPIRE].
[17] R. Gurau and J. P. Ryan, SIGMA **8**, 020 (2012) [arXiv:1109.4812 [hep-th]] [Search inSPIRE].
[18] N. Sasakura, Int. J. Mod. Phys. A **27**, 1250096 (2012) [arXiv:1203.0421 [hep-th]] [Search inSPIRE].
[19] R. L. Arnowitt, S. Deser, and C. W. Misner, Gen. Rel. Grav. **40**, 1997 (2008) [arXiv:gr-qc/0405109] [Search inSPIRE].
[20] J. Ambjorn, J. Jurkiewicz, and R. Loll; Phys. Rev. Lett. **93**, 131301 (2004) [arXiv:hep-th/0404156] [Search inSPIRE].
[21] D. Obster and N. Sasakura, Prog. Theor. Exp. Phys. **2018**, 043A01 (2018) [arXiv:1710.07449 [hep-th]] [Search inSPIRE].
[22] D. Obster and N. Sasakura, Eur. Phys. J. C **77**, 783 (2017) [arXiv:1704.02113 [hep-th]] [Search inSPIRE].
[23] N. Sasakura, Int. J. Mod. Phys. A **36**, 2150222 (2021) [arXiv:2104.11845 [hep-th]] [Search inSPIRE].
[24] B. Eynard, Counting Surfaces, Springer Basel, Basel (2016).
[25] D. J. Gross and E. Witten, Phys. Rev. D **21**, 446 (1980).
[26] S. R. Wadia, Phys. Lett. B **93**, 403 (1980).
[27] N. Sasakura, Prog. Theor. Exp. Phys. **2021**, 043A01 (2021) [arXiv:2008.07726 [hep-th]] [Search inSPIRE].
[28] N. Sasakura and Y. Sato, J. High Energy Phys. **10**, 109 (2015) [arXiv:1506.04872 [hep-th]] [Search inSPIRE].
[29] H. Chen, N. Sasakura, and Y. Sato, Phys. Rev. D **95**, 066008 (2017) [arXiv:1609.01946 [hep-th]] [Search inSPIRE].
[30] N. Sasakura and Y. Sato, Phys. Lett. B **732**, 32 (2014) [arXiv:1401.2062 [hep-th]] [Search inSPIRE].
[31] N. Sasakura, Int. J. Mod. Phys. A **28**, 1350111 (2013) [arXiv:1305.6389 [hep-th]] [Search inSPIRE].
[32] B. S. DeWitt, Phys. Rev. **160**, 1113 (1967).
[33] G. Narain, N. Sasakura, and Y. Sato, J. High Energy Phys. **01**, 010 (2015) [arXiv:1410.2683 [hep-th]] [Search inSPIRE].
[34] E. Witten, AMS/IP Stud. Adv. Math. **50**, 347 (2011) [arXiv:1001.2933 [hep-th]] [Search inSPIRE].
[35] D. Obster and N. Sasakura, Prog. Theor. Exp. Phys. **2020**, 073B06 (2020) [arXiv:2004.03152 [hep-th]] [Search inSPIRE].
[36] D. Obster and N. Sasakura, Universe **7**, 302 (2021) [arXiv:2107.10237 [gr-qc]] [Search inSPIRE].
[37] C. E. Berger, L. Rammelmüller, A. C. Loheac, and F. Ehmann, J. Braun, and J. E. Drut; Phys. Rep. **892**, 1 (2021) [arXiv:1907.10183 [cond-mat.quant-gas]] [Search inSPIRE].

Downloaded from https://academic.oup.com/ptep/article/2022/4/043A01/6547023 by Kyoto Daigaku Nogaku-bu Toshoshitsu user on 23 January 2023

[38] R. Neal, MCMC Using Hamiltonian Dynamics, in Handbook of Markov Chain Monte Carlo, eds. S. Brooks Brooks, A. Gelman Gelman, G. L. Jones Jones, and X.-L. Meng Meng, CRC Press, Boca Raton (2011), p. 113[arXiv:1206.1901 [stat.CO]] [Search inSPIRE].
[39] D. J. Earl and M. W. Deem, Phys. Chem. Chem. Phys. **7**, 3910 (2005).
[40] B. Dawes, D. Abrahams, and R. Rivera, Boost C++ Libraries (2021) available at: https://www.boost.org, (last accessed on 12 March 2022).
[41] L. Lionni and N. Sasakura, Prog. Theor. Exp. Phys. **2019**, 073A01 (2019) [arXiv:1903.05944 [hep-th]] [Search inSPIRE].
[42] N. Sasakura and S. Takeuchi, Eur. Phys. J. C **80**, 118 (2020) [arXiv:1907.06137 [hep-th]] [Search inSPIRE].
[43] T. Kawano, D. Obster, and N. Sasakura, Phys. Rev. D **97**, 124061 (2018) [arXiv:1805.04800 [hep-th]] [Search inSPIRE].
[44] H. S. Cohl, T. H. Dang, and T. M. Dunster, SIGMA **14**, 136 (2018) [arXiv:1803.07149 [math.AP]] [Search inSPIRE].
[45] S. Axler, *HFT.m* (2020) available at: https://www.axler.net/HFT_Math.html, (last accessed on 12 March 2022).
[46] S. A. Hartnoll, E. A. Mazenc, and Z. D. Shi, SciPost Phys. **7**, 081 (2019) [arXiv:1908.07058 [hep-th]] [Search inSPIRE].
[47] F. L. Hitchcock, J. Math. Phys. **6**, 164 (1927).
[48] J. D. Carroll and J.-J. Chang, Psychometrika **35**, 283 (1970).
[49] J. M. Landsberg, Tensors: Geometry and Applications, American Mathematical Society, Providence (2012).
[50] P. Comon, IEEE Sig. Proc. Mag. **31**, 44 (2014).
[51] C. J. Hillar and L. Lim, J. ACM **60**, 1 (2013) [arXiv:0911.1393 [cs.CC]] [Search inSPIRE].
[52] T. Castellani and A. Cavagna, J. Stat. Mech.: Theo. Exp. **2005**, 05012 (2005) [arXiv:cond-mat/0505032] [Search inSPIRE].
[53] G. Ni, L. Qi, F. Wang, and Y. Wang, J. Math. Anal. Appl. **329**, 1218 (2007).
[54] L. Qi, J. Math. Anal. Appl. **325**, 1363 (2007).
[55] D. Cartwright and B. Sturmfels, Lin. Alg. Appl. **438**, 942 (2013) [arXiv:1004.4953 [math.NA]] [Search inSPIRE].
[56] A. Crisanti and H.-J. Sommers, Z. Phys. B **87**, 341 (1992).
[57] National Institute of Standards and Technology, NIST Digital Library of Mathematical Functions, NIST, Gaithersburg, MD (2022) available at: http://dlmf.nist.gov/, (last accessed on 12 March 2022).

Downloaded from https://academic.oup.com/ptep/article/2022/4/043A01/6547023 by Kyoto Daigaku Nogaku-bu Toshoshitsu user on 23 January 2023